# A Novel and Functionally Diverse Class of Acetylcholine-gated Ion Channels

Iris Hardege *[1], Julia Morud *[1], Amy Courtney[1], William R Schafer [1,2]

**Affiliations**

[1] MRC Laboratory of Molecular Biology, Francis Crick Avenue, Cambridge, CB2 0QH, United Kingdom

[2] Department of Biology, KU Leuven, Leuven, Belgium

* These authors contributed equally to this work

Corresponding Author: William R Schafer, wschafer@mrc-lmb.cam.ac.uk

# Abstract

Fast cholinergic neurotransmission is mediated by acetylcholine-gated ion channels; in particular, excitatory nicotinic acetylcholine receptors play well established roles in virtually all nervous systems. Acetylcholine-gated inhibitory channels have also been identified in some invertebrate phyla, yet their roles in the nervous system are less well understood. We report the existence of multiple new inhibitory acetylcholine-gated ion channels with diverse ligand binding properties in *C. elegans*. We identify three channels, LGC-40, LGC-57 and LGC-58, whose primary ligand is choline rather than acetylcholine, as well as the first evidence of a truly polymodal channel, LGC-39, which is activated by both cholinergic and aminergic ligands. Using our newly deorphanised channel evidence we uncover the surprising extent to which a single neuron expresses both excitatory and inhibitory channels, not only for acetylcholine but also the other major neurotransmitters. The results presented in this study offer a new insight into the potential evolutionary benefit of a vast and diverse repertoire of LGICs to generate complexity in an anatomically compact nervous system.



# Keywords

Choline / *C. elegans* / Co-expression / Polymodal / Synaptic localisation


# Introduction

Rapid signalling through neuronal networks is essential for producing coordinated behaviours in animals. At the fundamental level, fast neuronal transmission is mediated through neurotransmitter release resulting in activation of ion channels on the postsynaptic neuron. In the textbook view, based predominately on mammalian systems, there are two major excitatory neurotransmitters, glutamate, and acetylcholine, and two inhibitory

neurotransmitters, GABA and glycine. Glutamate acts through a family of tetrameric ligand-gated cation channels, while the remaining neurotransmitters activate pentameric receptors from the Cys-loop receptor superfamily of ligand-gated ion channels (LGICs). Although LGICs are highly conserved across phyla, ligand binding properties and ion selectivity diverge significantly, resulting in a large diversity of mechanisms by which small molecules acting via LGICs can influence the activity in neuronal circuits.

Despite their conserved general structure, Cys-loop LGICs vary significantly in their functional properties, particularly when channels from invertebrate phyla are considered. For example, insects and nematodes express inhibitory glutamate receptors from the Cys-loop superfamily, localised both in neurons and muscles, which are targets of the anthelminthic drug ivermectin (Cully et al., 1996, 1994). Many animals including insects, nematodes and mammals also express LGICs which can be gated by aminergic ligands, including histamine-gated chloride channels (Gisselmann et al., 2002), important for fly visual processing, a number of nematode channels, involved in learning and motor control (Morud et al., 2021; Pirri et al., 2009), as well as the excitatory mammalian 5-$HT_3$ receptor (Kondo et al., 2014; Lombaert et al., 2018). Even more divergent roles for LGICs have been identified in marine species, where LGICs gated by terpenes and chloroquine function as chemoreceptors in octopus (van Giesen et al., 2020).

Cys-loop channels can be subdivided into two large clades, the first containing the nicotinic receptors and their paralogues including the 5-$HT_3$ receptors, and the other containing channels more closely related to $GABA_A$ receptors (Jones and Sattelle, 2008). The *C. elegans* genome contains several subfamilies which appear to have diversified independently from vertebrate channels during evolution, leading to the existence of several nematode specific

50 LGIC subfamilies. The *C. elegans* genome contains a number of $GABA_A$-like subfamilies,
51 including genes encoding both anion and cation-selective channels (Jobson et al., 2015; Margie
52 et al., 2013; Putrenko et al., 2005; Ranganathan et al., 2000; Ringstad et al., 2009; Yassin et
53 al., 2001). One of these subfamilies consist of genes for both anion and cation selective
54 monoamine-gated channels, another of acetylcholine-gated anion channels or channels that are
55 still largely uncharacterised. One member in one of these subgroups, LGC-40, has previously
56 been reported to be a low affinity serotonin-gated channel also gated by acetylcholine and
57 choline (Ringstad et al., 2009). The properties of the remaining channels in these subgroups,
58 including their ligands, ion selectivity, and expression patterns, are currently unknown.
59
60 Here we describe the deorphanisation and characterisation of five new *C. elegans*
61 LGICs activated by acetylcholine. One of these, LGC-39, forms a polymodal homomeric anion
62 channel activated by acetylcholine as well as by monoamines, while the others are activated by
63 choline and/or acetylcholine. Using public single cell RNAseq expression data together with
64 our new electrophysiological data, we also predict the polarity of synapses in the worm
65 connectome, as well as intracellular localisation patterns for uncharacterised LGICs. These
66 results highlight the unexpected functional diversity of cholinergic signalling in the *C. elegans*
67 nervous system.
68

69 # Results

70 **Deorphanisation of Uncharacterised LGICs Reveals Diversity of Cholinergic Channels**

71 The *C. elegans* genome encodes a diverse superfamily of pentameric ligand-gated ion
72 channels (LGICs), of which several subfamilies are poorly characterised. Here we investigate
73 the diverse group, which consists of 3 subgroups named after a channel from each group; the
74 LGC-45 group, the LGC-41 group, and the GGR-1 group (here renamed to LGC-57 group)

75 (Figure 1B) and contains many channels whose activating ligand and function are unknown.
76 To investigate the properties of these channels, we first expressed each channel gene in
77 *Xenopus* oocytes and tested for current activation during the perfusion of a panel of
78 neurotransmitters. Despite their homology to vertebrate $GABA_A$ and glycine receptors (the
79 source of the name GGR-1), we observed no activation of any members of the LGC-57 group
80 (or any diverse group channels) by either GABA or glycine. Instead, we found three closely
81 related channels of the LGC-57 group: LGC-57 (formerly GGR-1), LGC-58 (formerly GGR-
82 2) and LGC-40 to be specifically gated by choline and acetylcholine (Figure 1A). All three
83 channels showed a preference for choline, with $EC_{50}$ values 2.5 to 3-fold lower for choline than
84 acetylcholine (Figure 1C). These findings parallel a previous report that LGC-40 forms a
85 choline and acetylcholine-gated channel, although in contrast to that report we did not observe
86 serotonin responses (Ringstad et al., 2009). We did not observe currents in response to any of
87 the tested compounds for the remaining members of the diverse group (Figure S1A). The lack
88 of agonist induced currents may be because the channel was poorly expressed, the correct
89 ligand was not tested or because they function only as components of heteromeric complexes.
90 The remaining member of the LGC-57 group, LGC-39 showed unusual activation properties
91 which will be discussed below.
92
93 In addition to the diverse group channels, many other *C. elegans* LGICs lack identified
94 ligands. For example, while several members of the ACC group (Acetylcholine-gated Chloride
95 Channels) of LGICs have been shown to form acetylcholine-gated chloride channels, four
96 members of this subfamily *(acc-4, lgc-47, lgc-48,* and *lgc-49)* had not previously been
97 characterised (Figure 1B, in red). Upon expression in *Xenopus* oocytes, we found that one of
98 these channels, LGC-49, formed a homomeric acetylcholine-gated channel with an $EC_{50}$ of
99 19$\mu$M (Figure 1C), similar to the $EC_{50}$ values published for other members of this group

100 (Putrenko et al., 2005; Takayanagi-Kiya et al., 2016). Unlike the members of the LGC-57
101 group, which showed activation by both acetylcholine and choline, LGC-49 showed no
102 significant activation by choline. None of the ligands tested here induced currents for ACC-4,
103 LGC-47 or LGC-48, either alone, or in combination with closely related and previously
104 characterised LGICs, such as ACC-1 (Figure S1A&C) (Putrenko et al., 2005). Given the vast
105 number of possible heteromeric combinations within the ACC group it may be that these
106 orphan channels are part of more complex channel compositions not tested here.

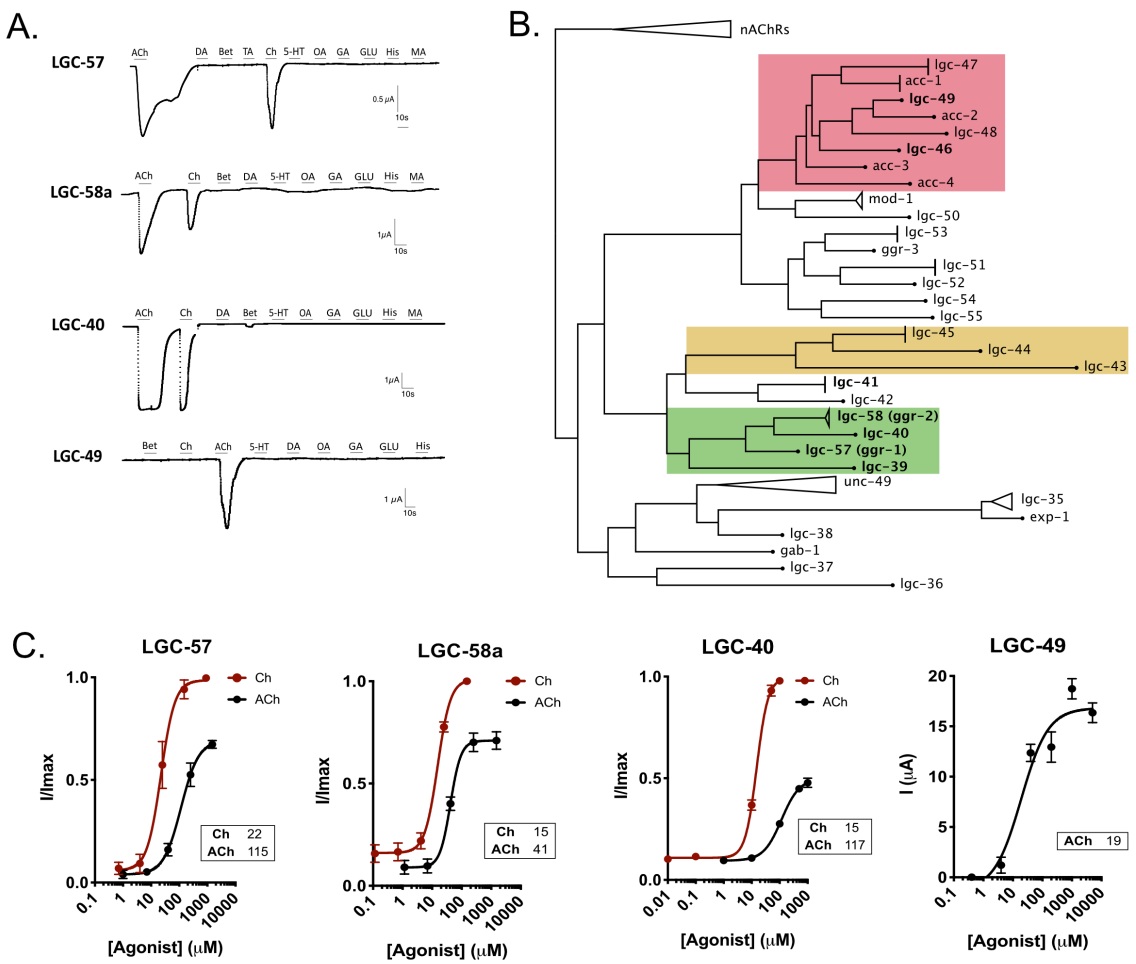


107

108 **Figure 1. Deorphanisation of Cholinergic Ligand-Gated Ion Channels.** (**A**) Continuous current traces of
109 *Xenopus* oocytes expressing LGC-57, LGC-58a, LGC-40, and LGC-49, oocytes were perfused for 10s with a
110 panel of ligands each at 1mM: ACh (acetylcholine), Ch (choline), Bet (betaine), TA (tyramine), DA (dopamine),
111 5-HT (serotonin), OA (octopamine), GA (GABA), GLU (glutamate), His (histamine), MA (melatonin). (**B**)

112 Phylogenetic tree of a subgroup of Cys-loop ligand gated ion channels in *C. elegans*, groups of interest are
113 highlighted by colour: 'ACC' group of acetylcholine gated channels (red), LGC-45 group (yellow), LGC-41 group
114 (blue), LGC-57 group (green). (**C**) Dose response curves for LGC-57, LGC-58a, LGC-40 and LGC-49 in response
115 to their major ligand(s). Current is normalised by I/Imax for each oocyte, for LGC-49 current is raw un-normalised
116 current. Error bars represent SEM of 5-14 oocytes. Curves are fitted with a four-parameter variable slope, inserts
117 show $EC_{50}$ in $\mu$M for each ligand.
118
119 We next investigated the ion selectivity of the newly-deorphanised channels by
120 carrying out ion substitution experiments in oocytes expressing LGC-57, LGC-58, LGC-40, or
121 LGC-49. For all these channels we observed significant reversal potential shifts following
122 substitution of standard high NaCl buffer for low Cl (Na Gluconate), but not following
123 substitution with $Na^+$-free (NMDG) solution, indicating selectivity for anions over cations for
124 all the tested channels (Figure 2A-B). We also tested the previously deorphanised channel
125 LGC-46 (Liu et al., 2017), which to date lacked ion selectivity data. This channel likewise
126 showed reversal shifts characteristic of an anion selective channel (Figure 2A-B). Interestingly,
127 all members of the LGC-57 group possess a PAR motif (Proline-Alanine-Arginine), located in
128 the M2-3 intracellular loop (Figure S1B), which has been shown to impart anion selectivity to
129 LGICs (Wotring et al., 2003). Although several uncharacterised members of the ACC group
130 have sequences that diverge from the PAR motif, both LGC-49 and LGC-46 contain the PAR
131 motif sequence (Figure S1B). Thus, the PAR motif appears to correlate with anion selectivity
132 in both the LGC-57 and ACC groups of nematode acetylcholine-gated LGICs.
133
134 **Cholinergic Channels Display Diverse Antagonist Binding Properties**
135 To understand if there are further functional differences between the channels
136 deorphanised in this study, we exposed each channel to three cholinergic antagonists,
137 mecamylamine, strychnine and d-tubocurarine. Strychnine and d-tubocurarine have been

138 shown to compete with the full agonist for the ligand binding domain, although their binding
139 mechanisms vary between LGICs of different classes (Brams et al., 2011); in contrast,
140 mecamylamine has been shown to interact with the transmembrane regions of mammalian
141 nAChRs (Bondarenko et al., 2014). Indeed, we saw that the antagonistic profile differed
142 significantly between the newly-deorphanised channels. For example, within the LGC-57
143 group the two smallest antagonists, mecamylamine and strychnine, had similar $IC_{50}$ values for
144 LGC-57, LGC-58a and LGC-40 (Figure 2D). However, tubocurarine, the largest molecule of
145 the antagonists, displayed an 11-fold shift in $IC_{50}$ for LGC-57 compared to LGC-58 and LGC-
146 40 (Figure 2D). Thus, the binding capabilities of tubocurarine on LGC-57 differs substantially
147 from that of its closest family members LGC-58 and LGC-40. Likewise, in the ACC group,
148 LGC-46 and LGC-49 could both be blocked by mecamylamine, strychnine and tubocurarine
149 (Figure 2D). These dissimilarities again highlight the discrete differences between channels
150 from the same subfamily, which may have similar ligand-binding profiles for endogenous
151 ligands. Interestingly, tubocurarine was the most potent blocker for the ACC group channels
152 LGC-46 and LGC-49, whereas this antagonist was the least effective of the channels tested in
153 the LGC-57 group.
154
155 We also tested the channels' responses to repeated stimulation by their primary ligand.
156 We found LGC-40 to be sensitive to repeated stimulation, displaying a significant difference
157 in ratio between the first and second pulse after both 10s of and 60s of washing intervals (Figure
158 2C). In contrast, all other channels were capable of fast activation intervals as they did not
159 display any decrease in peak amplitude after repeated stimulation (Figure 2C). Thus, LGC-40
160 appears to desensitise more than the other channels following activation by its ligand.

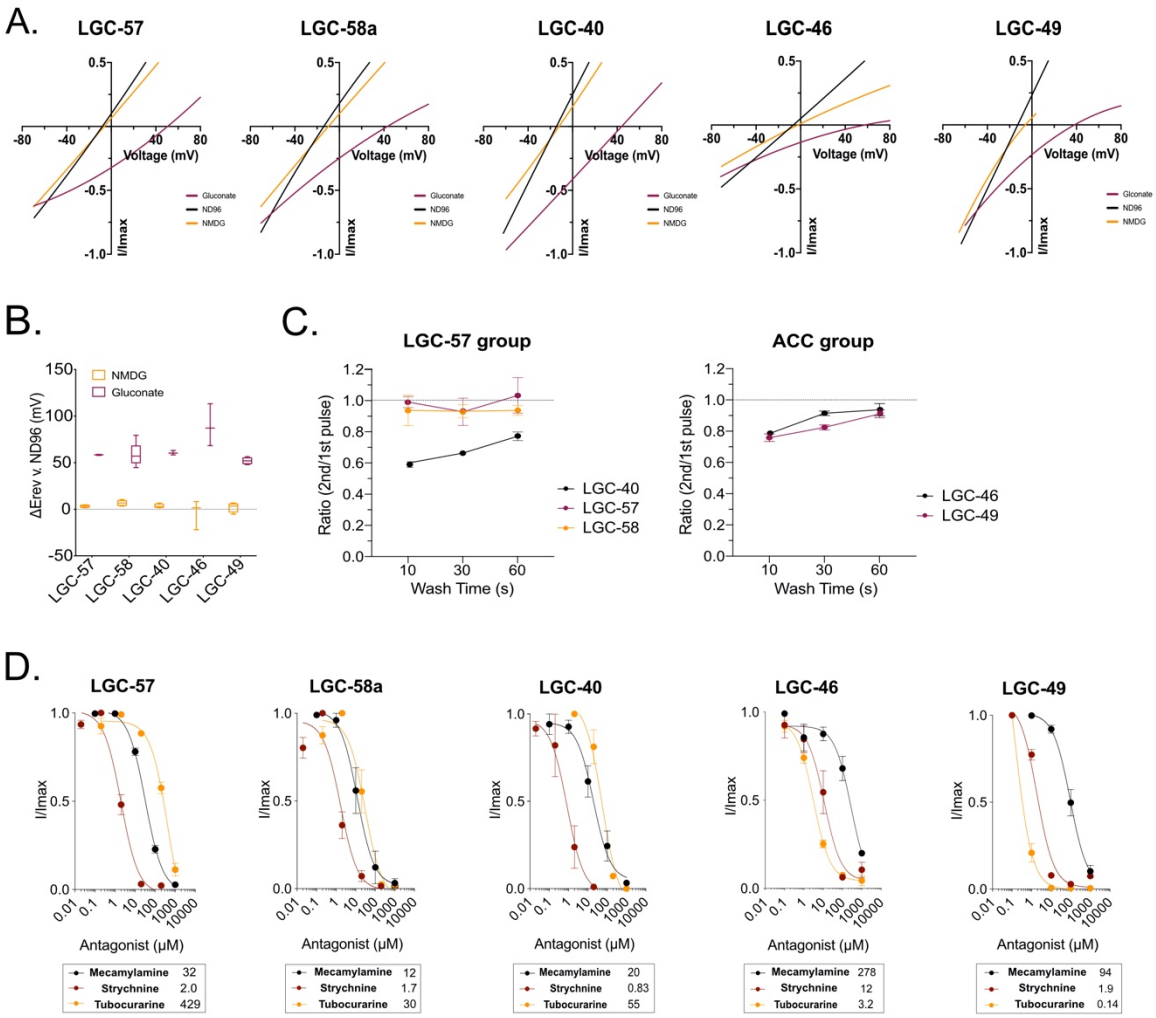


**Figure 2. Ion Selectivity and Antagonistic Characterisation of Cholinergic LGICs.** (**A**) Representative current voltage plots of newly deorphanised channels in ND96, Na gluconate or NMDG solutions. Current was normalised by leak current subtraction (in absence of activating ligand) and the peak current for each oocyte. (**B**) Box plot of $\Delta E_{rev}$ of NMDG and Na Gluconate vs. ND96 in oocytes expressing LGC-57, LGC-58a, LGC-40, LGC-39, LGC-46, and LGC-49, $E_{rev}$ was calculated in the presence of the major agonist of each channel and leak subtracted. N=6-11 oocytes. (**C**) Current ratio of oocytes expressing LGC-57, LGC-58, LGC-46, LGC-49 or LGC-39 undergoing repeated agonist application with 10s, 30s and 60s wash intervals. Error bars represent SEM. N=5-9 oocytes per condition. (**D**) Antagonist application in the presence of ligands using mecamylamine, strychnine and tubocurarine. Current was normalised by I/Imax for each oocyte, curves are fitted with a three-parameter variable slope, error bars represent SEM of 2-7 oocytes, inserts show $IC_{50}$ in $\mu$M for each antagonist.

173 **LGC-39 is a Novel Polymodal Channel Activated by Cholinergic and Aminergic**
174 **Ligands**

175 One channel from the LGC-57 group, LGC-39, showed distinct ligand binding
176 properties from the rest of the group. Unlike the other LGC-57 subfamily members, LGC-39
177 showed relatively little activation by choline (Figure 3A). Moreover, while acetylcholine
178 activated LGC-39 strongly (with an $EC_{50}$ of 1290$\mu$M), the most potent ligands for LGC-39
179 were the monoamines octopamine and tyramine (with $EC_{50}$ values of 921$\mu$M and 686$\mu$M
180 respectively; Figure 3A-B). In addition, LGC-39 also displayed small currents in response to
181 dopamine (Figure 3A). Both activation by aminergic or cholinergic ligands resulted in a
182 sigmoidal shaped dose response curve, which would indicate that all ligands bind in a similar
183 positive cooperative manner in the same pocket (Cattoni et al., 2015). Like other members of
184 the LGC-57 family, LGC-39 contains the PAR sequence (Figure S1B), and LGC-39-
185 expressing oocytes showed reversal potential shifts in response to chloride but not sodium
186 substitution (Figure 3C). Thus, *lgc-39* appears to encode a homomeric anionic and polymodal
187 channel, capable of being activated by both aminergic and cholinergic neurotransmitters
188 (Figure 3A-C).
189

190 We tested the effects of antagonists on LGC-39 currents evoked by different activating
191 ligands. In the presence of acetylcholine, LGC-39 could be blocked by the antagonists
192 mecamylamine, strychnine and tubocurarine (Figure 3D). In contrast, the octopamine response
193 could not be blocked by mecamylamine or strychnine. Surprisingly, strychnine, without the
194 presence of an activating ligand, acted as a partial agonist, since it induced a small current with
195 an $EC_{50}$ of 7.5$\mu$M (Figure 3D). To further separate the functionality of the ligands, we also
196 investigated if repeated activation by the different ligands influenced the ability for reactivation
197 of LGC-39 differently (Figure 3E). No difference was seen for any wash interval between the

198 ligands, which could suggest that all ligands occupy the binding site in a similar time frame or

199 that the recovery time for the receptor is independent of the activating ligand.

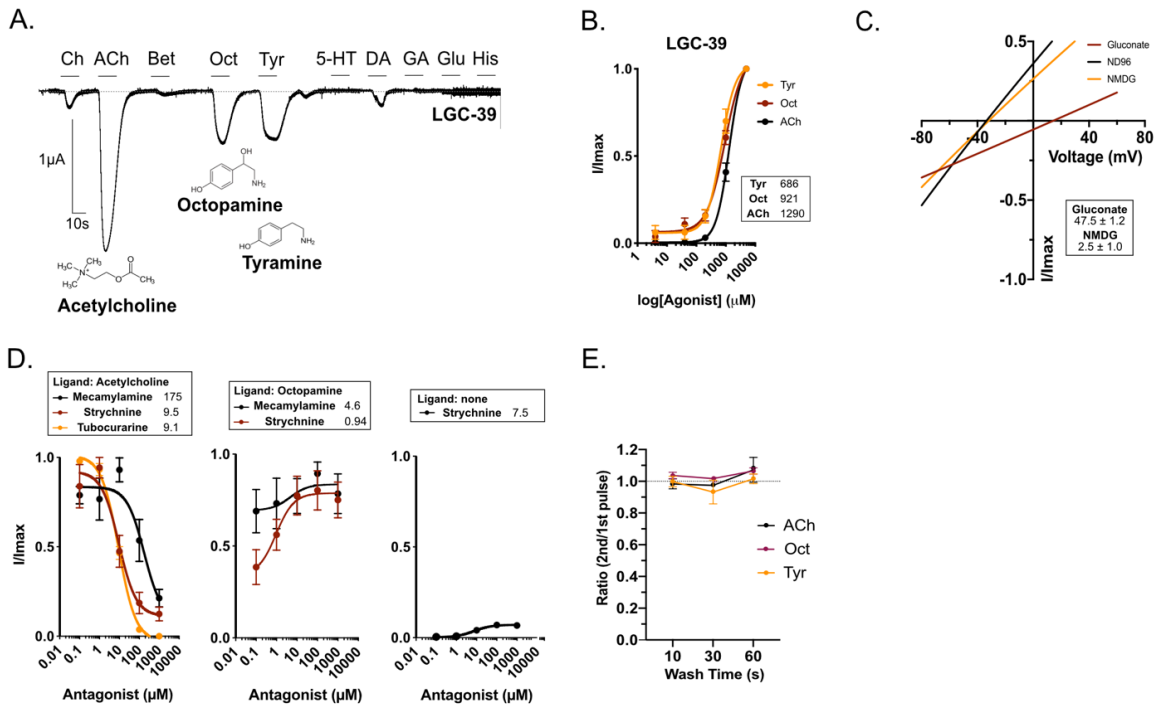


200

201 **Figure 3. LGC-39 Forms a Polymodal Ligand-Gated Ion Channel.** (**A**) Continuous current trace of a *Xenopus*

202 oocyte clamped at -60mV expressing LGC-39, perfused during 10s pulses with a panel of ligands each at 1mM:

203 ACh (acetylcholine), Ch (choline), Bet (betaine), Tyr (tyramine), DA (dopamine), 5-HT (serotonin), Oct

204 (octopamine), GA (GABA), Glu (glutamate), His (histamine). (**B**) Dose response curve for LGC-39 in response

205 to ACh, Oct and Tyr. Current is normalised by I/Imax for each oocyte. Error bars represent SEM of 8-12. Curves

206 are fitted using a four-parameter variable slope, inserts show $EC_{50}$ in $\mu$M for each ligand. (**C**) Current-voltage

207 relationship during recordings in NMDG, Na Gluconate or ND96 in oocytes expressing LGC-39. Insert shows

208 $\Delta E_{rev}$ vs. ND96 in mV +/- SEM of 5 oocytes. (**D**) Antagonist dose response curves for LGC-39 expressing oocytes

209 activated by either ACh, Oct or no ligand at a constant dose and varying the antagonist doses (mecamylamine,

210 strychnine and tubocurarine). Error bars represent SEM of 3-7 oocytes. Curves are fit with a three-parameter

211 variable slope, inserts show $IC_{50}$ in $\mu$M for each ligand. (**E**) Three different agonists do not differ in how they

212 influence the ability for LGC-39 to be stimulated with short time intervals after repeated stimulation.

213

214 **Cholinergic Channels show Broad and Varied Expression in The *C. elegans* Nervous**

215 **System**

216 To gain insight into the roles of cholinergic LGICs in the nervous system, we generated
217 reporter lines to characterise their neural expression patterns. We used a similar set of
218 fluorescent reporter lines to characterise the expression pattern of the newly deorphanised
219 LGICs, by using transcriptional reporter transgenes in which the upstream promoter of the *lgc*
220 gene drives the expression of a fluorescent protein. We then identified transgene-expression
221 based upon location, morphology and known marker lines. Using such a transcriptional
222 reporter, we observed primarily neuronal expression of the genes in the LGC-57 group, with
223 little overlap observed in the neurons that were expressing reporters for *lgc-40*, *lgc-57* and *lgc-*
224 *58* (Figure 4A-C). *lgc-40* was expressed in many pharyngeal neurons (M2, M3, MC, MI, I2),
225 *lgc-57* in the A-class and B-class motorneurons of the ventral cord, and *lgc-58* in the egg-laying
226 motorneurons (VCs; *lgc-57* was also observed in a subset of VCs). This suggests that these
227 channels are likely to exist primarily as homomers *in vivo* and function in distinct target
228 neurons. Further we observed the reporter for *lgc-39* in a range of interneurons and motor
229 neurons, including the AVA premotor interneurons (Figure 4E). In addition to receiving
230 extensive cholinergic input, the AVA neurons are the major synaptic target for the only
231 octopaminergic neurons, the RICs, suggesting that LGC-39 may be exposed to both
232 octopamine and acetylcholine *in vivo* (Figure 4F) and may be involved in both cholinergic and
233 octopaminergic synaptic transmission. Finally, we found that the ACC group channel, *lgc-49,*
234 was expressed in sensory neurons, including posterior sensory neurons such as ALN and PLN
235 (Figure 4D).

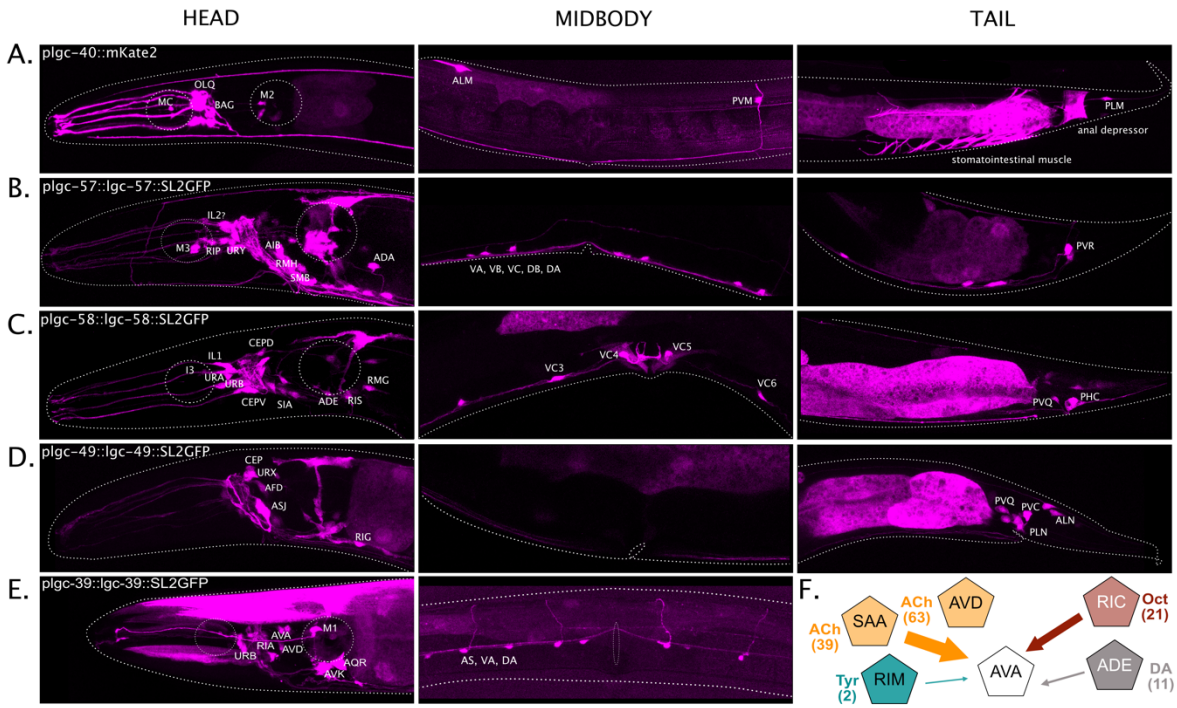


**Figure 4. Newly Deorphanised LGICs are Expressed Broadly in the Nervous System. (A-E)** Fluorescent reporters of intercistonically spliced mKate2 or GFP driven under the promoter and/or genomic sequence of reveals broad neuronal expression of cholinergic channels with little overlap. (**F**) Schematic depicting a subset of the synaptic connections received by the *lgc-39* expressing neuron class, AVA, numbers in brackets show the total number of synapses for each connection.

We also used reporters to analyse the expression pattern of several still-orphan LGICs, from the diverse and ACC groups, including *lgc-42, lgc-47, lgc-48, lgc-43* and *lgc-45*, as well as the previously deorphanised acetylcholine-gated channel *lgc-46* (Takayanagi-Kiya et al., 2016) (Figure S2A-D). These reporters also showed diverse and distinct patterns of expression, primarily in neurons. For example, *lgc-46* was broadly expressed in several neurons, mostly in the head (Figure S2D). Most of the orphan channels were also expressed specifically in neurons; for *lgc-47* this expression was unusually broad, encompassing sensory, motor, and interneurons (Figure S2A), while *lgc-48* was expressed only in a single pair of neurons, the ADL chemosensory neurons (Figure S2B). Interestingly, the two orphan channels, *lgc-43,* and

252 *lgc-45,* which lack a PAR sequence and may thus encode cationic channels (Figure S1B), did
253 not appear to be expressed in neuronal tissue, but instead in the hypodermis (Figure S2B).
254 Together, these data suggest that these channels play various roles in, and outside, the nervous
255 system.
256
257 **Excitatory and Inhibitory ACh Receptors are Co-expressed in Many Neurons**
258 Our fluorescent reporter expression analysis indicated that many of the newly
259 deorphanised inhibitory ACh-gated receptors in this study are expressed in neurons previously
260 shown to also express excitatory ACh-gated channels (Barbagallo et al., 2010; Raizen et al.,
261 1995). These results imply that acetylcholine, as an inhibitory neurotransmitter, may have a
262 larger role than previously appreciated, and that acetylcholine contributes to both inhibitory
263 and excitatory events in many neurons. To determine the extent to which excitatory and
264 inhibitory receptors, for the same neurotransmitter, are expressed in individual neural classes,
265 we made use of the single cell RNAseq dataset from *C. elegans* neurons (Taylor et al., 2021).
266 We first generated a complete list of ionotropic receptors for each of the three classical
267 neurotransmitters ACh, GABA and glutamate (Table S1). Since receptors with unknown
268 ligand-identity would have the potential to bias predictions, we predicted the ligand and ion
269 selectivity of orphan channels based upon homology with closely related characterised
270 channels, and the presence, or absence, of a PAR motif in the M2-3 intracellular loop (see
271 Methods).
272
273 From this analysis, we found a remarkable frequency of neural classes that co-express
274 both inhibitory and excitatory receptors for the same neurotransmitter. This was particularly
275 notable for acetylcholine, for which over 60% of the neural classes expressed both excitatory
276 and inhibitory ACh receptors. In contrast, GABA receptors were more biased toward

277 inhibition, with over 40% of neural classes expressing only inhibitory GABA receptors (Figure
278 5A, S3). To make generalised predictions of synaptic polarity, we summed expression of
279 inhibitory and excitatory receptors, for each neurotransmitter, in each neural class and assigned
280 synapse polarity based on the most prevalent receptors in each neural class, assuming that all
281 receptors in a cell are present equally at all synapses (Figure 5C, S4). This analysis suggested
282 that the majority of ACh and glutamate synapses are excitatory and most GABA synapses are
283 inhibitory, though this varied significantly for individual connections (Figure 5B).
284
285 To examine the validity of our polarity predictions we investigated the sign prediction
286 using previously characterised neuronal circuits. We picked the well-studied locomotion circuit
287 (Chalfie et al., 1985) consisting of the interneurons AVD, AVE and AVA, which initiate
288 reversals, and PVC and AVB that initiate forward movement. Most of our predicted connection
289 polarities (Figure 5D) were consistent with circuit data from previous studies, such as the
290 excitatory connection between AVA and the VA and DA motor neurons, which is involved in
291 controlling reverse locomotion, as well as the excitatory connection from the sensory neuron
292 ASH to the reverse command neuron AVA (Mellem et al., 2002; Piggott et al., 2011). We also
293 observed connections which appeared counter intuitive such as an inhibitory acetylcholine
294 connection from AVD to AVA, two interneuron pairs thought to be co-ordinately active during
295 reverse locomotion (Faumont et al., 2012) (Figure 5D). While some studies have proposed
296 additional inhibitory connections within this circuit (Rakowski and Karbowski, 2017), AVA
297 neurons express several ACh-gated channels and has a relatively low ratio of inhibitory to
298 excitatory receptor expression (1:3), upon which this prediction was made. This suggests that
299 some connections may indeed be both inhibitory and excitatory, especially where a neuron
300 expresses a large range of different channels and receives input from many different neural

classes. Connections such as these require further *in vivo* investigations to address these predictions.

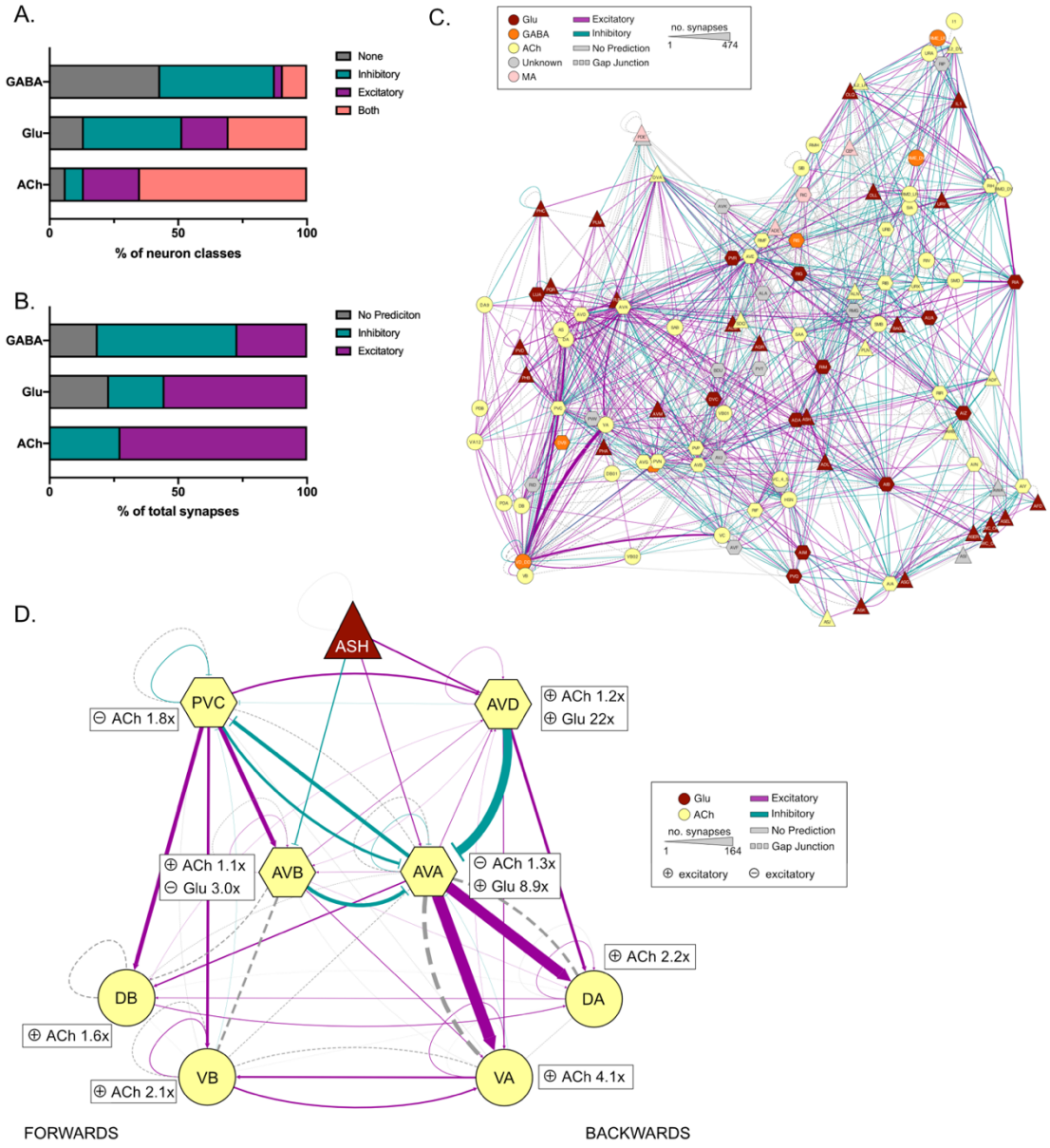


**Figure 5. Predicting Synapse Polarity Based on LGIC Expression.** (**A**) Bar chart depicting the percentage of total neuron classes expression inhibitory, excitatory, both or no receptors for GABA, glutamate (Glu) and acetylcholine (ACh). (**B**) Bar chart depicting the percentage of total synapses for a given neurotransmitter that are predicted to be inhibitory, excitatory or have no prediction. (**C**) Network diagram depicting the polarity of synaptic connections between neural classes, connection colour show polarity: teal (inhibitory), pink (excitatory), grey (no prediction). Gap junctions are represented in dashed lines. Line weight represents number of synapses and nodes are coloured by the major neurotransmitter a class release. Diagram made with cytoscape

311 using the EntOpt clustering package. (**D**) Network diagram depicting the predicted polarity of the locomotion
312 circuit, connection colour shows polarity: teal (inhibitory), pink (excitatory), grey (no prediction). Inserts next to
313 each neuron node show the fold magnitude of expression of the major receptor type for each neurotransmitter in
314 each neural class, e.g., AVA neurons express 1.3x as many inhibitory ACh receptors than excitatory and 8.9x as
315 many excitatory glutamate receptors than inhibitory. Gap junctions are represented by dashed lines. Line weight
316 represents number of synapses and nodes are coloured by the major neurotransmitter a class release. Diagram
317 made with cytoscape.

318 **Determining Synaptic Localisation of LGICs**

319 We reasoned that the single cell RNAseq dataset (Taylor et al., 2021) might also be
320 useful for predicting the intracellular localisation of cholinergic LGICs, as presynaptic
321 receptors would be predicted to be expressed in cholinergic neurons, while postsynaptic
322 receptors should be expressed in neurons receiving cholinergic input. To assess the correlation
323 between the number of cholinergic synapses a neuron makes ('outgoing ACh synapses') or
324 receives ('incoming ACh synapses'), with the expression level of cholinergic LGICs, we
325 produced two heatmaps showing the expression of ACh-gated receptors, with neural classes
326 ranked by the total number of incoming or outgoing ACh synapses (Figure 6A-B). This
327 analysis highlights that the expression of some ACC group channels, in particular, *lgc-46,*
328 correlate with both the number of incoming and outgoing ACh synapses (Figure 6C-D & Figure
329 S5). This correlation suggests that these receptors may be acting either pre- or post-
330 synaptically. In contrast, members of the choline and ACh-gated LGC-57 group, *lgc-57*, *lgc-*
331 *58* and *lgc-40*, showed little correlation with either incoming or outgoing synapses (Figure 6C-
332 D). Surprisingly for this subgroup, several cells with high ACh connectivity showed low
333 receptor expression level (Figure 6C-D). This may be suggestive of an extrasynaptic role for
334 these receptors, however further evidence is required to make these assumptions.

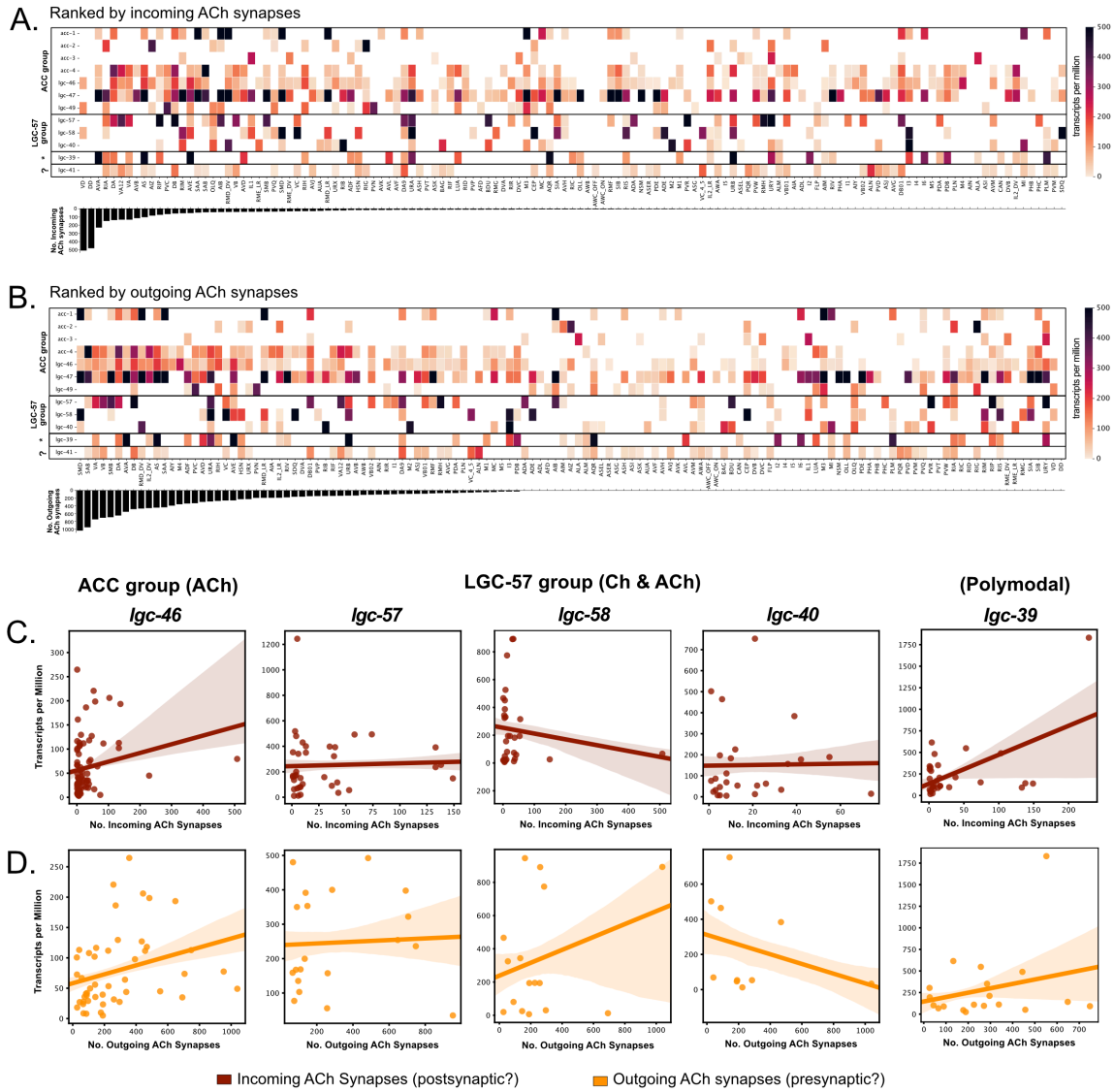


**Figure 6. Correlation of Cholinergic Synapses with Expression Pattern of Cholinergic Ion Channels.** (**A-B**) Heatmaps showing the expression level of newly deorphanised LGICs in each neural class. Neurons are sorted by the total number of cholinergic synapses they receive (top, 'Incoming') or make (bottom, 'Outgoing'). (**C & D**) Scatter plots showing correlation between the total number of incoming (red) or outgoing (orange) cholinergic synapses for a given neuronal class and expression of *lgc-46*, *lgc-57*, *lgc-58*, *lgc-40*, and *lgc-39*.

To empirically assess the synaptic localisation of cholinergic LGICs, we generated endogenous GFP-tagged CRISPR lines for members of the LGC-57 subgroup, including *lgc-39*, *lgc-40*, *lgc-57*, and *lgc-58* and (Figure 7A-D). In all cases GFP was inserted in the intracellular M3/4 loop and the function of the resulting chimeric protein was verified in

346 *Xenopus* oocytes (Figure S6A). We observed a clear difference in the localisation pattern for
347 these channels. LGC-39::GFP was localised in distinct punctate structures both in the nerve
348 ring and along the ventral cord, suggestive of synaptic localisation (Figure 7A), and consistent
349 with the positive correlation between *lgc-39* expression and incoming and outgoing ACh
350 synapses (Figure 6A-D). Members of the choline-gated LGC-57 group however showed
351 diffuse protein expression. LGC-40::GFP appeared to have diffuse expression in the nerve ring,
352 and touch receptor neurons, with cell bodies often being visible (Figure 7B). Notably, cell body
353 LGC-40::GFP expression was detected in the posterior and anterior bulbs, in cells which
354 anatomically correspond to MC and M2 neurons (Figure 7B). While LGC-57::GFP appeared
355 to have overall low expression and little protein localisation could be seen above background
356 (Figure 7C). LGC-58::GFP was clearly visible in the nerve ring and VC4/5, including some
357 punctate structures (Figure 7D). Since these choline-sensitive members of the LGC-57 group
358 showed little correlation with ACh synapses, their diffuse protein localisation may be
359 indicative of an extrasynaptic role (Figure 6C & Figure 7D).

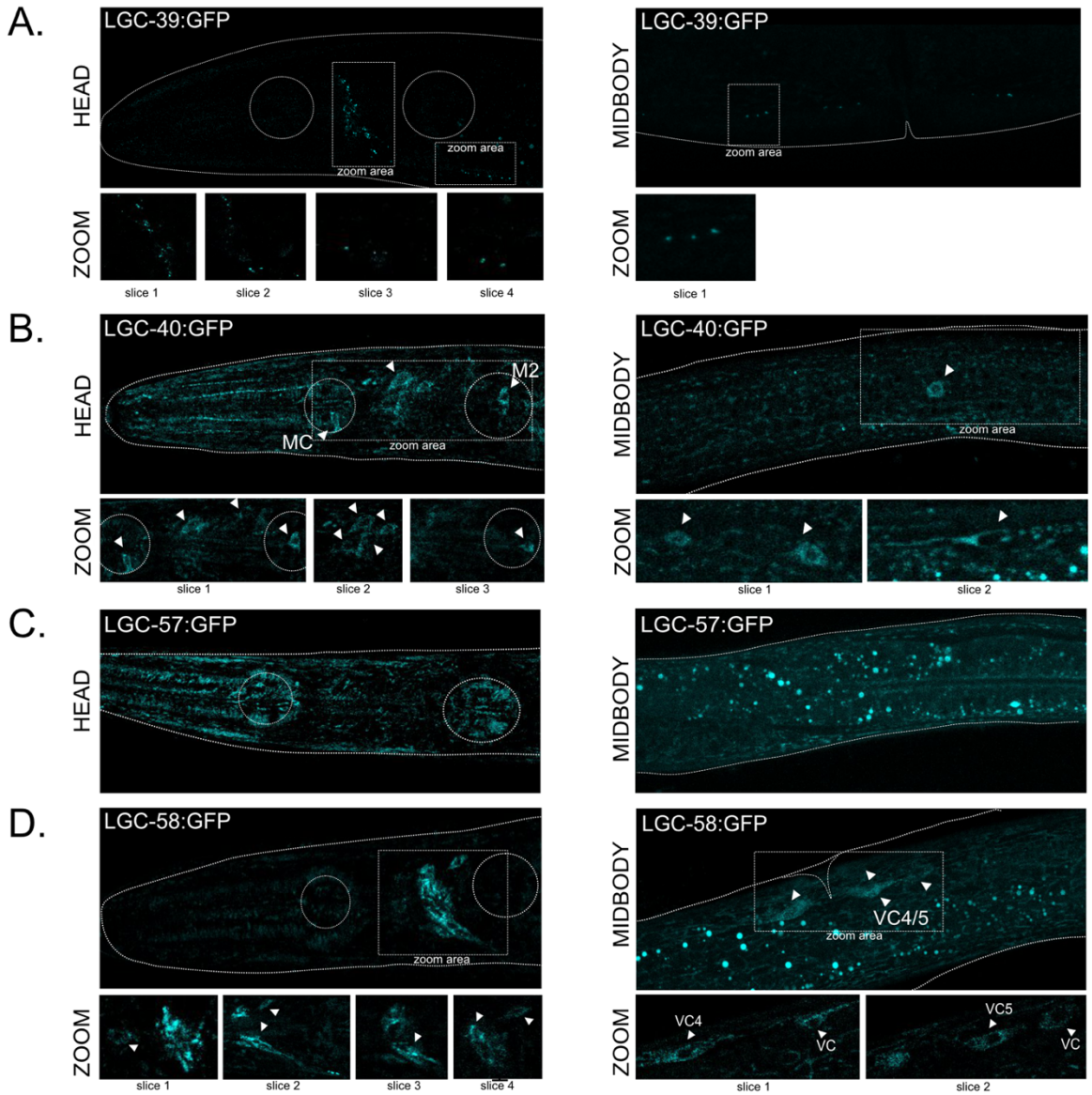


**Figure 7. Protein expression pattern of cholinergic ion channels.** (**A-D**) Localisation of endogenously GFP tagged LGC-39, LGC-40, LGC-57 and LGC-58. White arrows highlight areas of interest, represented in higher magnification below.

# Discussion

## A Novel Family of Cholinergic LGICs

This study highlights the diversity among cholinergic LGICs in *C. elegans*. Nematodes have previously been shown to express acetylcholine and choline-gated excitatory LGICs

369 related to nicotinic receptors, as well as inhibitory acetylcholine-gated chloride in the ACC
370 group. Here we describe a second inhibitory subfamily, that contains channels gated by both
371 choline and acetylcholine: LGC-57, LGC-58 (previously named GGR-1 and GGR-2) and
372 LGC-40. In contrast to the ACC group of acetylcholine-gated anion channels, these newly
373 deorphanised channels are gated preferentially by choline, the metabolite of acetylcholine
374 which is abundant at cholinergic synapses.
375
376 These results add to the already extensive catalogue of acetylcholine-gated channels in
377 *C. elegans* (Putrenko et al., 2005; Takayanagi-Kiya et al., 2016), and to the growing number
378 of choline-gated channels described in *C. elegans,* which previously consisted of the excitatory
379 DEG-3/DES-2 channel found within the nAChR superfamily (Yassin et al., 2001). Together
380 with our new data this highlights the expansion and importance of cholinergic transmission in
381 nematodes. These newly deorphanised channels display subtle variations in their ability to bind
382 ligands and antagonists, which translates into physiologically relevant differences that may
383 increase the fine tuning in the control of neuronal transmission and contribute to complex
384 neuronal signalling within a relatively minimal neuronal network. Interestingly, the
385 electrophysiologically similar channels LGC-57, LGC-58, and LGC-40 show largely distinct
386 patterns of expression within the nervous system of *C. elegans*, suggesting they may form
387 homomeric channels with distinct functions *in vivo*. When tagged with a fluorescent protein,
388 these three channels also showed a diffuse localisation pattern within the neuron, suggesting
389 that in contrast to the ACC group channels, such as LGC-46 (Takayanagi-Kiya et al., 2016),
390 these channels may not be synaptically localised. This suggests a possible distinct extrasynaptic
391 role for choline by acting via these channels, in the modulation of the nervous system.
392

393 The observation that choline shows higher efficacy for these channels, a molecule
394 generated at cholinergic synapses through catabolism of acetylcholine by cholinesterases,
395 raises the possibility that choline is their true *in vivo* ligand and that choline itself may function
396 as a neuromodulator. The idea that choline could activate cholinergic receptors differently from
397 acetylcholine has been discussed for other cholinergic receptors that can be dose-dependently
398 blocked or activated by choline (Purohit and Grosman, 2006). Here we have identified
399 cholinergic receptors in which choline act as a full agonist, showing preference in binding and
400 activation degree for choline over acetylcholine. Previous reports suggest aromatic residues in
401 the extracellular domain of mammalian neuromuscular AChRs play a vital part in stabilising
402 the binding of acetylcholine over the binding to choline (Bruhova and Auerbach, 2017).
403 Interestingly, at least some of these aromatic residues are lacking in the choline-gated receptors
404 identified here. Thus, it is not unreasonable to hypothesise that choline could be an authentic
405 endogenous ligand for these channels in *vivo*.
406
407 **A Polymodal LGIC Activated by Both Aminergic and Cholinergic Ligands**
408 In this study we also identified a novel polymodal channel, LGC-39, which was gated
409 not only by acetylcholine, but also by the aminergic ligands tyramine and octopamine. We
410 observed dose-dependent activation of LGC-39 channels by these structurally distinct ligand
411 classes of endogenous ligands at similar, physiologically-relevant concentrations. The
412 expression pattern of *lgc-39* suggests that the channel might be exposed to all these ligands *in*
413 *vivo*; for example, *lgc-39* is highly expressed in the AVA premotor neurons, which receive a
414 large amount of input from acetylcholine producing neurons (White, 1986), as well as from the
415 RIC neurons, the only octopamine producing cells in the *C. elegans* nervous system (Alkema
416 et al., 2005). The AVA neurons also receive some input from tyraminergic and dopaminergic
417 neurons, transmitters which we also found can activate LGC-39. Interestingly, in contrast to

418 the choline-gated channels LGC-40, LGC-57, and LGC-58, we observe clear punctate
419 localisation of LGC-39 in both the nerve ring and along the ventral cord, with no fluorescence
420 visible in the cell bodies. This may suggest a role for LGC-39 as postsynaptic receptor for both
421 cholinergic and aminergic neurotransmission.
422
423 The concept of a truly polymodal receptor, that can be activated by structurally diverse
424 compounds, has not before been investigated in great detail, though previous observations have
425 described roles for receptors that can use dual ligands for allosteric modulation (Cummings
426 and Popescu, 2015). For example, dopamine exhibits a pseudo competitive ability to
427 antagonise $GABA_A$ currents, although this effect cannot be blocked by competitive $GABA_A$
428 antagonists, which bind the main binding pocket (Hoerbelt et al., 2015). Further, D-serine has
429 been shown to function as an allosteric modulator of NMDA receptor activity (Wolosker and
430 Balu, 2020). In contrast to these examples, based on their capability to achieve dose-dependent
431 activation by both amines and acetylcholine, both groups of neurotransmitters appear to be true
432 ligands of LGC-39, most likely interacting with the ligand-binding domain. Understanding the
433 mechanisms by which these multiple neurotransmitters can activate LGC-39 and potentially
434 affect different behavioural outputs will be of interest in future studies.
435
436 **Functional Insights into The *C. elegans* Connectome**
437 With increasing molecular and physiological characterisation of neurotransmitter
438 receptors in *C. elegans*, it is becoming feasible to more accurately predict the functionality of
439 synapses in the *C. elegans* connectome. In this study we used the expression pattern of newly
440 and previously deorphanised LGICs for the three classical neurotransmitters, ACh, glutamate
441 and GABA, to predict the polarity of synapses in the *C. elegans* connectome. By assigning
442 synapse polarity based on relative expression levels of anionic and cationic receptors, we have

443 provisionally predicted the sign of chemical synapses involving classical neurotransmitters.
444 Although similar attempts to assign polarity to *C. elegans* synapses have been made in the past
445 (Fenyves et al., 2020), these predictions were based upon incomplete or incorrect ligand
446 assignment for many LGICs. These revised predictions correlate well with experimental data
447 for many well-characterised circuits, such as the excitatory connections between the ASH
448 nociceptors and the AVA interneurons, as well as between the AVAs and the VA and DA
449 motorneurons (Mellem et al., 2002; Piggott et al., 2011). Our predicted inhibitory connection
450 between AVB and AVA interneurons also correspond well with empirical data on the
451 locomotor circuit (Kawano et al., 2011; Qi et al., 2012). In addition to providing sign
452 predictions for synaptic connections, our model also provides a ratio of excitatory to inhibitory
453 expression for each neuronal class and neurotransmitter. Not only do our predictions generate
454 interesting functional hypotheses for future investigation, but this additional information also
455 allows these predictions to be critically assessed. It also raises the question whether these
456 connections, with low receptor ratios, represent truly complex connections, a question that
457 could be addressed in future studies.
458
459 A surprising outcome of the expression analysis was the high frequency with which
460 individual neurons expressed cationic and anionic receptors for the same neurotransmitter. This
461 was especially prevalent for acetylcholine; our analysis indicated that 60% of neural classes
462 express both inhibitory and excitatory receptors for acetylcholine, 30% for glutamate and 10%
463 for GABA. One explanation for this apparent paradox is that excitatory and inhibitory receptors
464 might be differentially localised in neurons, with some found extrasynaptically and others
465 enriched in synapses. Various *C. elegans* LGICs are known to act in regions other than the
466 post-synapse; for example, *lgc-35* has been shown to mediate GABA spill-over transmission
467 (Jobson et al., 2015), while *lgc-46* appears be localised to the pre-synapse as an autoreceptor

468 (Takayanagi-Kiya et al., 2016). The choline-sensitive channels from the LGC-57 group
469 likewise appear to be extrasynaptic in their localisation (Figure 7). In addition, postsynaptic
470 sites might themselves contain a mixture of excitatory and inhibitory receptors, which could
471 differ in their ligand affinity, desensitisation kinetics and regulation. Indeed, LGIC localisation
472 is not static; for example, glutamatergic AMPA receptors have been shown in many species to
473 increase their synaptic localisation during learning (Malinow and Malenka, 2002), and recent
474 evidence indicates that *C. elegans* LGICs also display regulated membrane trafficking upon
475 learning (Morud et al., 2021). Thus, *C. elegans* may contain large numbers of complex
476 cholinergic synapses with the potential to be excitatory or inhibitory depending on context or
477 experience.
478

479 # Materials and Methods

480 ## *C. elegans* culture

481 Unless otherwise specified, *C. elegans* worms were cultured on NGM agar plates with OP50
482 (Stiernagle, 2006). A full list of strains used in this study can be found in table S1.
483

484 ## *Xenopus laevis* oocytes

485 Defolliculated *Xenopus laevis* oocytes were obtained from EcoCyte Bioscience (Dortmund,
486 Germany) and in ND96 (in mM: 96 NaCl, 1 $MgCl_2$, 5 HEPES, 1.8 $CaCl_2$, 2 KCl) solution at
487 16° C for 3-7 days.

488 ## Molecular biology

489 Unless otherwise specified, cDNA sequences of *C. elegans* genes were cloned from wildtype
490 N2 worm cDNA (generated by reverse transcription PCR from total worm RNA using Q5
491 polymerase (New England Biosciences)). Where multiple isoforms are present isoform a was

492 used. LGC-39 cDNA was generated by gene synthesis (ThermoFischer). For expression in
493 *Xenopus* oocytes, ion channel cDNA sequences were cloned into the KSM vector downstream
494 of a T3 promoter and between *Xenopus* β-globin 5' and 3'UTR regions using the HiFi assembly
495 protocol (New England Biosciences). *C. elegans* expression constructs were also generated
496 using the HiFi assembly protocol (New England Biosciences) into the pDESTR4R3II
497 backbone. *C. elegans* gDNA sequences were cloned from wildtype N2 gDNA and expression
498 verified by the addition of GFP or mKate2 introduced on the same plasmid after an
499 intercistronic splice site (SL2 site). Unless otherwise specified promoter sequences consist of
500 approximately 2kb of gDNA upstream of the start codon.
501

502 **CRISPR/CAS9-mediated gene manipulation**

503 Endogenous tagging of the M3/4 cytosolic loop of *C. elegans* LGIC proteins with GFP was
504 carried out either using the SapTrap protocol (Dickinson et al., 2018; Schwartz and
505 Jorgensen, 2016) for *lgc-39(lj121)*, or by SunyBiotech (Fuzhou, China) for *lgc-57(syb3536)*,
506 *lgc-58(syb3562)*, and *lgc-40(syb3594)*.
507

508 **RNA synthesis and microinjection**

509 CRNA was synthesised *in vitro* using the T3 mMessage mMachine transcription kit according
510 to manufacturer's protocol to include a 5' cap (ThermoFischer Scientific). Prior to injection
511 RNA was purified using the GeneJET RNA purification kit (Thermo Fischer Scientific). Size
512 sorted and defolliculated *Xenopus* oocytes (Ecocyte) were placed individually into 96-well
513 plates and injected with 50 nL of 500 ng/$\mu$L RNA using the Roboinject system (Multi Channel
514 Systems GmbH). When two constructs were co-injected the total RNA concentration remained
515 500 ng/$\mu$L, with a 1:1 ratio of the components. Injected oocytes were incubated at 16°C in
516 ND96 until the day of recording, typically between 3-6 days post injection.

517

518 **Two-Electrode Voltage Clamp (TEVC) recording and data analysis**

519 Two-electrode voltage clamp recordings were carried out using either the Robocyte2 system
520 or a manual set up with an OC-725D amplifier (Multi Channel Systems GmbH). Glass
521 electrodes with a resistance ranging from 0.7-2 MΩ were pulled on a P1000 Micropipette Puller
522 (Sutter). Electrodes contained AgCl wires and backfilled with a 1.5M KCl and 1 M acetic
523 mixture. Unless otherwise stated, oocytes were clamped at -60mV. Continuous recordings at
524 500Hz were taken during application of a panel of agonists or antagonists. Data was recorded
525 using the RoboCyte2 control software, or with WinWCP for manual recordings, and filtered at
526 10 Hz.

527

528 Dose response protocols used 10s agonist application pulses with 60s of wash in ND96 between
529 each dose. Data was gathered over at least two occasions, using different batches of oocytes.
530 Peak current for each dose was normalised to the oocyte maximum current using a custom-
531 built python script (Morud et al., 2021). Normalised data was imported into Graphpad (Prism)
532 and fitted to either a three or four parameter nonlinear Hill equation to obtain the highest degree
533 of fit and calculate the $EC_{50}$. Antagonist dose responses and ion selectivity recordings were
534 carried out using the $EC_{50}$ concentration of the primary agonist. Antagonist dose response
535 protocols used 10s agonist + antagonist windows, with 60s of ND96 washes between doses.
536 The agonist concentrations remained constant. Antagonist $IC_{50}$ values were calculated using a
537 second custom-built python script (Morud et al., 2021). Normalised data was imported into
538 Graphpad (Prism) and fitted to either a three or four parameter nonlinear Hill equation to obtain
539 the highest degree of fit and calculate the $IC_{50}$.

540

541 Ion selectivity was detected using a voltage ramp protocol from -80mV to +60mV (20mV/s)
542 in the presence of the primary agonist in three different solutions: ND96, NMDG ($Na^+$ free) and

543 Na Gluconate (low $Cl^-$) solutions. Data was normalised to max current and $\Delta E_{Rev}$ was calculated
544 using a custom-built python script (Morud et al., 2021). The resulting individual values or
545 mean, SD and n for each construct was imported in GraphPad for further plotting and statistical
546 analysis. Statistically significant differences in $\Delta E_{Rev}$ were calculated in GraphPad using a two-
547 way ANOVA with Tukey's correction for multiple comparisons. A representative normalised
548 trace for each construct was also generated in Graphpad.
549

550 **Confocal and Cell ID**

551 Worms were prepared and immobilised with 75 mM NaAzide in M9 and mounted onto 2%
552 agarose in M9 pads. Image stacks were acquired with a 63x water immersion lens on a Leica
553 SP8 or STED or using a 40x oil immersion objective on a Zeiss LSM780. Collapsed z-stack
554 images were generated in Fiji/Image J. Neurons expressing fluorescent reporters were
555 identified by cell shape, position and crossing with the multicolour reference worm NeuroPAL
556 (Yemini et al., 2020).
557

558 **Synaptic polarity prediction**

559 Inhibitory and excitatory chemical synapse prediction for ACh, Glu and GABA synapses were
560 based upon expression levels of appropriate LGICs in postsynaptic cells. Chemical and
561 electrical connectome data was obtained from Wormweb (http://wormweb.org/details.html),
562 LGIC expression data was taken from the Cengen project using threshold level 4 (Taylor et al.,
563 2021), ligand and ion selectivity for each channel was based upon this work. Previous work
564 and predictions are presented in Table 1. Binary expression of LGICs for each neurotransmitter
565 in each neural class were based upon expression and characterised in four groups: only
566 excitatory, only inhibitory, both excitatory and inhibitory or none. These binary values were
567 used to make the binary expression heatmap. Overall polarity of a synapse was calculated by

568 summing the expression of all inhibitory and all excitatory LGICs for a given neurotransmitter
569 in each cell class. The sum inhibitory was then taken from the sum of excitatory expression,
570 resulting in an overall positive or negative signed expression in each neural class for each
571 neurotransmitter. The ratio of these sums was also calculated to indicate the strength of
572 polarity. It was assumed that each LGIC in each neural class is present equally at all synapses,
573 therefore each incoming connection could be assigned a polarity based upon its receptor
574 expression for that neurotransmitter. The resulting network with polarity was imported into
575 cystoscope (Shannon et al., 2003) for plotting and further analysis. Analysis scripts can be
576 found on GitHub at hiris25/Worm-Connectome-Polarity.
577

578 **Expression and cholinergic synapse analysis**

579 The total number of cholinergic input or output synapses was calculated for each neural class
580 by summing the number of presynapses for each cell that received a synapse from an ACh-
581 producing neuron (incoming synapses), or the total number of post-synapses an ACh-
582 producing neural class makes (outgoing synapses). Acetylcholine producing cells were
583 described by (Pereira et al., 2015), the assumption was that all synapses made by an ACh-
584 producing cell also release ACh, even when this cell co-transmits another neurotransmitter.
585 Synapse number for each neuron was taken from (White, 1986). Expression data was obtained
586 from (Taylor et al., 2021) using a threshold of 2. Neural classes were sorted by ACh in or out
587 degree and the expression of each gene was mapped using a heatmap with an upper threshold
588 of 500. For correlation plots, cells that did not express a receptor, were removed from the
589 analysis. Correlation between expression level and ACh in, or out, degree was mapped using
590 relplot in python's seaborn package, confidence intervals were placed at 68%, corresponding
591 to the standard error of the estimate.
592

593 **Data Availability**

594 Python scripts can be found at on GitHub at hiris25/TEVC-analysis-scripts and hiris25/Worm-
595 Connectome-Polarity. Aggregated data used for analysing TEVC data are available upon
596 request from the Lead Contact. Further information and requests for *C. elegans* strains and
597 plasmids is to be sent to and will be fulfilled by the Lead Contact William R Schafer,
598 wschafer@mrc-lmb.cam.ac.uk

599

600 **Acknowledgements**

601 The authors gratefully acknowledge Denise Walker and Lidia Ripoll Sanchez for help with
602 cloning design, help with generating and maintaining strains, and other past and present
603 members of the Schafer lab for helpful discussions. We would like to acknowledge the Centre
604 for Cellular Imaging at the University of Gothenburg, Sweden, and the National Microscopy
605 Infrastructure, NMI (NMI01125), for providing imaging facilities. This work was supported
606 by grants from the Medical Research Council (MC-A023-5PB91), the Wellcome Trust
607 (WT103784MA), National Institute of Health (W.R.S.), the Swedish Research council
608 (VR2017-00236), Knut and Alice Wallenberg foundation (KAW2019,0293), Bollan stipend,
609 Lundgrenska stiftelserna and Magnus Bergvalls Stiftelse (J.M.).

610

611 **Author Contributions**

612 I.H., J.M. and W.R.S. designed the experiments. I.H., J.M., performed experiments and
613 analysed data. I.H., J.M. and W.R.S. wrote the manuscript and all authors read and critically
614 revised the manuscript to its final form.

615

616 **Conflicts of Interest**

617 The authors declare no competing interests.

618

619 # References


620 Alkema MJ, Hunter-Ensor M, Ringstad N, Horvitz HR. 2005. Tyramine functions
621 independently of octopamine in the Caenorhabditis elegans nervous system. *Neuron* **46**.
622 doi:10.1016/j.neuron.2005.02.024

623 Barbagallo B, Prescott HA, Boyle P, Climer J, Francis MM. 2010. A dominant mutation in a
624 neuronal acetylcholine receptor subunit leads to motor neuron degeneration in
625 Caenorhabditis elegans. *J Neurosci* **30**. doi:10.1523/JNEUROSCI.1515-10.2010

626 Bondarenko V, Targowska-Duda KM, Jozwiak K, Tang P, Arias HR. 2014. Molecular
627 interactions between mecamylamine enantiomers and the transmembrane domain of the
628 human α4β2 nicotinic receptor. *Biochemistry* **53**. doi:10.1021/bi400969x

629 Brams M, Pandya A, Kuzmin D, van Elk R, Krijnen L, Yakel JL, Tsetlin V, Smit AB, Ulens
630 C. 2011. A structural and mutagenic blueprint for molecular recognition of strychnine
631 and d-tubocurarine by different Cys-loop receptors. *PLoS Biol* **9**.
632 doi:10.1371/journal.pbio.1001034

633 Bruhova I, Auerbach A. 2017. Molecular recognition at cholinergic synapses: acetylcholine
634 versus choline. *J Physiol* **595**. doi:10.1113/JP273291

635 Cattoni DI, Chara O, Kaufman SB, Flecha FLG. 2015. Cooperativity in binding processes:
636 New insights from phenomenological modeling. *PLoS One* **10**.
637 doi:10.1371/journal.pone.0146043

638 Chalfie M, Sulston JE, White JG, Southgate E, Nichol Thomson J, Brenner S. 1985. The
639 neural circuit for touch sensitivity in Caenorhabditis elegans. *J Neurosci* **5**.
640 doi:10.1523/jneurosci.05-04-00956.1985

641 Cully DF, Paress PS, Liu KK, Schaeffer JM, Arena JP. 1996. Identification of a Drosophila

642 melanogaster glutamate-gated chloride channel sensitive to the antiparasitic agent
643 avermectin. *J Biol Chem*. doi:10.1074/jbc.271.33.20187
644 Cully DF, Vassilatis DK, Liu KK, Paress PS, Van Der Ploeg LHT, Schaeffer JM, Arena JP.
645 1994. Cloning of an avermectin-sensitive glutamate-gated chloride channel from
646 Caenorhabditis elegans. *Nature*. doi:10.1038/371707a0
647 Cummings KA, Popescu GK. 2015. Glycine-dependent activation of NMDA receptors. *J Gen*
648 *Physiol* **145**. doi:10.1085/jgp.201411302
649 Dickinson D, Slabodnick M, Chen A, Goldstein B. 2018. SapTrap assembly of repair
650 templates for Cas9-triggered homologous recombination with a self-excising cassette.
651 *microPublication Biol* **2018**. doi:10.17912/W2KT0N
652 Faumont S, Lindsay TH, Lockery SR. 2012. Neuronal microcircuits for decision making in
653 C. elegans. *Curr Opin Neurobiol*. doi:10.1016/j.conb.2012.05.005
654 Fenyves BG, Szilágyi GS, Vassy Z, Sőti C, Csermely P. 2020. Synaptic polarity and sign-
655 balance prediction using gene expression data in the Caenorhabditis elegans chemical
656 synapse neuronal connectome network. *PLoS Comput Biol* **16**.
657 doi:10.1371/journal.pcbi.1007974
658 Gisselmann G, Pusch H, Hovemann BT, Hatt H. 2002. Two cDNAS coding for histamine-
659 gated ion channels in D. melanogaster. *Nat Neurosci*. doi:10.1038/nn787
660 Hoerbelt P, Lindsley TA, Fleck MW. 2015. Dopamine directly modulates GABAA receptors.
661 *J Neurosci* **35**. doi:10.1523/JNEUROSCI.4390-14.2015
662 Jobson MA, Valdez CM, Gardner J, Garcia LR, Jorgensen EM, Beg AA. 2015. Spillover
663 transmission is mediated by the excitatory GABA receptor LGC-35 in C. elegans. *J*
664 *Neurosci*. doi:10.1523/JNEUROSCI.4557-14.2015
665 Jones AK, Sattelle DB. 2008. The cys-loop ligand-gated ion channel gene superfamily of the
666 nematode, Caenorhabditis elegans. *Invertebr Neurosci* **8**:41–47. doi:10.1007/s10158-

667 008-0068-4
668 Kawano T, Po MD, Gao S, Leung G, Ryu WS, Zhen M. 2011. An imbalancing act: Gap
669 junctions reduce the backward motor circuit activity to bias C. elegans for forward
670 locomotion. *Neuron* **72**. doi:10.1016/j.neuron.2011.09.005
671 Kondo M, Nakamura Y, Ishida Y, Yamada T, Shimada S. 2014. The 5-HT3A receptor is
672 essential for fear extinction. *Learn Mem* **21**. doi:10.1101/lm.032193.113
673 Liu P, Chen B, Mailler R, Wang ZW. 2017. Antidromic-rectifying gap junctions amplify
674 chemical transmission at functionally mixed electrical-chemical synapses. *Nat Commun*.
675 doi:10.1038/ncomms14818
676 Lombaert N, Hennes M, Gilissen S, Schevenels G, Aerts L, Vanlaer R, Geenen L, Van
677 Eeckhaut A, Smolders I, Nys J, Arckens L. 2018. 5-HTR 2A and 5-HTR 3A but not 5-
678 HTR 1A antagonism impairs the cross-modal reactivation of deprived visual cortex in
679 adulthood. *Mol Brain* **11**. doi:10.1186/s13041-018-0404-5
680 Malinow R, Malenka RC. 2002. AMPA receptor trafficking and synaptic plasticity. *Annu Rev*
681 *Neurosci*. doi:10.1146/annurev.neuro.25.112701.142758
682 Margie O, Palmer C, Chin-Sang I. 2013. C. elegans chemotaxis assay. *J Vis Exp*.
683 doi:10.3791/50069
684 Mellem JE, Brockie PJ, Zheng Y, Madsen DM, Maricq A V. 2002. Decoding of polymodal
685 sensory stimuli by postsynaptic glutamate receptors in C. elegans. *Neuron* **36**.
686 doi:10.1016/S0896-6273(02)01088-7
687 Morud J, Hardege I, Liu H, Wu T, Choi M-K, Basu S, Zhang Y, Schafer WR. 2021.
688 Deorphanization of novel biogenic amine-gated ion channels identifies a new serotonin
689 receptor for learning. *Curr Biol*. doi:10.1016/j.cub.2021.07.036
690 Pereira L, Kratsios P, Serrano-Saiz E, Sheftel H, Mayo AE, Hall DH, White JG, LeBoeuf B,
691 Garcia LR, Alon U, Hobert O. 2015. A cellular and regulatory map of the cholinergic

692 nervous system of C. Elegans. *Elife* **4**. doi:10.7554/eLife.12432
693 Piggott BJ, Liu J, Feng Z, Wescott SA, Xu XZS. 2011. The neural circuits and synaptic
694 mechanisms underlying motor initiation in C. elegans. *Cell* **147**.
695 doi:10.1016/j.cell.2011.08.053
696 Pirri JK, McPherson AD, Donnelly JL, Francis MM, Alkema MJ. 2009. A Tyramine-Gated
697 Chloride Channel Coordinates Distinct Motor Programs of a Caenorhabditis elegans
698 Escape Response. *Neuron* **62**. doi:10.1016/j.neuron.2009.04.013
699 Purohit Y, Grosman C. 2006. Block of muscle nicotinic receptors by choline suggests that the
700 activation and desensitization gates act as distinct molecular entities. *J Gen Physiol* **127**.
701 doi:10.1085/jgp.200509437
702 Putrenko I, Zakikhani M, Dent JA. 2005. A family of acetylcholine-gated chloride channel
703 subunits in Caenorhabditis elegans. *J Biol Chem* **280**. doi:10.1074/jbc.M412644200
704 Qi YB, Garren EJ, Shu X, Tsien RY, Jin Y. 2012. Photo-inducible cell ablation in
705 Caenorhabditis elegans using the genetically encoded singlet oxygen generating protein
706 miniSOG. *Proc Natl Acad Sci U S A* **109**. doi:10.1073/pnas.1204096109
707 Raizen DM, Lee RYN, Avery L. 1995. Interacting genes required for pharyngeal excitation
708 by motor neuron MC in Caenorhabditis elegans. *Genetics* **141**.
709 doi:10.1093/genetics/141.4.1365
710 Rakowski F, Karbowski J. 2017. Optimal synaptic signaling connectome for locomotory
711 behavior in Caenorhabditis elegans: Design minimizing energy cost. *PLoS Comput Biol*
712 **13**. doi:10.1371/journal.pcbi.1005834
713 Ranganathan R, Cannon SC, Horvitz HR. 2000. MOD-1 is a serotonin-gated chloride channel
714 that modulates locomotory behaviour in C. elegans. *Nature* **408**. doi:10.1038/35044083
715 Ringstad N, Abe N, Horvitz HR. 2009. Ligand-gated chloride channels are receptors for
716 biogenic amines in C. Elegans. *Science (80- )* **325**. doi:10.1126/science.1169243

717 Schwartz ML, Jorgensen EM. 2016. SapTrap, a toolkit for high-throughput CRISPR/Cas9
718 gene modification in Caenorhabditis elegans. *Genetics* **202**.
719 doi:10.1534/genetics.115.184275
720 Shannon P, Markiel A, Ozier O, Baliga NS, Wang JT, Ramage D, Amin N, Schwikowski B,
721 Ideker T. 2003. Cytoscape: A software Environment for integrated models of
722 biomolecular interaction networks. *Genome Res* **13**. doi:10.1101/gr.1239303
723 Stiernagle T. 2006. Maintenance of C. elegans. *WormBook*. doi:10.1895/wormbook.1.101.1
724 Takayanagi-Kiya S, Zhou K, Jin Y. 2016. Release-dependent feedback inhibition by a
725 presynaptically localized ligand-gated anion channel. *Elife*. doi:10.7554/eLife.21734
726 Taylor SR, Santpere G, Weinreb A, Barrett A, Reilly MB, Xu C, Varol E, Oikonomou P,
727 Glenwinkel L, McWhirter R, Poff A, Basavaraju M, Rafi I, Yemini E, Cook SJ, Abrams
728 A, Vidal B, Cros C, Tavazoie S, Sestan N, Hammarlund M, Hobert O, Miller DM. 2021.
729 Molecular topography of an entire nervous system. *Cell* **184**.
730 doi:10.1016/j.cell.2021.06.023
731 van Giesen L, Kilian PB, Allard CAH, Bellono NW. 2020. Molecular Basis of Chemotactile
732 Sensation in Octopus. *Cell*. doi:10.1016/j.cell.2020.09.008
733 White JG. 1986. The structure of the nervous system of the nematode Caenorhabditis
734 elegans. *Philos Trans R Soc London B, Biol Sci* **314**:1–340. doi:10.1098/rstb.1986.0056
735 Wolosker H, Balu DT. 2020. d-Serine as the gatekeeper of NMDA receptor activity:
736 implications for the pharmacologic management of anxiety disorders. *Transl Psychiatry*.
737 doi:10.1038/s41398-020-00870-x
738 Wotring VE, Miller TS, Weiss DS. 2003. Mutations at the GABA receptor selectivity filter:
739 A possible role for effective charges. *J Physiol* **548**. doi:10.1113/jphysiol.2002.032045
740 Yassin L, Gillo B, Kahan T, Halevi S, Eshel M, Treinin M. 2001. Characterization of the
741 DEG-3/DES-2 receptor: A nicotinic acetylcholine receptor that mutates to cause

742 neuronal degeneration. *Mol Cell Neurosci* **17**. doi:10.1006/mcne.2000.0944

743 Yemini E, Lin A, Nejatbakhsh A, Varol E, Sun R, Mena GE, Samuel ADT, Paninski L,

744 Venkatachalam V, Hobert O. 2020. NeuroPAL: A Multicolor Atlas for Whole-Brain

745 Neuronal Identification in C. elegans. *Cell*. doi:10.1016/j.cell.2020.12.012

746

747 # Supplementary Tables and Figure with Legends

| Gene | Gated | Pos/Neg | Inferred? | Ref |
|---|---|---|---|---|
| *acr-2* | ACh | P | | [1] |
| *acr-3* | ACh | P | | [1] |
| *acr-6* | ACh | P | yes | |
| *acr-7* | ACh | P | yes | |
| *acr-8* | ACh | P | yes | |
| *acr-9* | ACh | P | yes | |
| *acr-10* | ACh | P | yes | |
| *acr-11* | ACh | P | yes | |
| *acr-12* | ACh | P | | [2] |
| *lev-8* | ACh | P | | [3] |
| *acr-14* | ACh | P | yes | |
| *acr-15* | ACh | P | yes | |
| *acr-16* | ACh | P | | [4] |
| *acr-19* | ACh | P | yes | |
| *acr-25* | ACh | P | yes | |
| *eat-2* | ACh | P | | [5] |
| *lev-1* | ACh | P | | [6] |
| *unc-29* | ACh | P | | [6] |
| *unc-38* | ACh | P | | [6] |
| *unc-63* | ACh | P | | [7] |
| *unc-49* | GABA | N | | [8] |
| *exp-1* | GABA | P | | [9] |
| *lgc-35* | GABA | P | | [10] |
| *lgc-36* | GABA | P | yes | |
| *lgc-37* | GABA | N | yes | |
| *lgc-38* | GABA | N | yes | |
| *avr-14* | Glu | N | | [11] |
| *avr-15* | Glu | N | | [11] |
| *glc-1* | Glu | N | | [12] |
| *glc-2* | Glu | N | | [13] |

| | | | | |
|---|---|---|---|---|
| *glc-3* | Glu | N | | [14] |
| *glc-4* | Glu | N | yes | |
| *acc-2* | ACh | N | | [15] |
| *acc-3* | ACh | N | | [15] |
| *acc-4* | ACh | P | yes | |
| *lgc-46* | ACh | N | | [16] |
| *lgc-47* | ACh | N | yes | |
| *lgc-48* | ACh | P | yes | |
| *lgc-49* | ACh | N | | This study |
| *ggr-1/lgc-57* | choline, ACh | N | | This study |
| *ggr-2/lgc-58* | choline, ACh | N | | This study |
| *lgc-39* | ACh, tyramine, octopamine | N | | This study |
| *lgc-40* | choline, ACh | N | | This study |
| *gab-1* | GABA | N | | [17] |
| *acc-1* | ACh | N | | [15] |
| *nmr-1* | Glu | P | | [18] |
| *nmr-2* | Glu | P | | [19] |
| *glr-1* | Glu | P | | [20] |
| *glr-2* | Glu | P | | [20] |
| *glr-3* | Glu | P | Yes | |
| *glr-4* | Glu | P | Yes | |
| *glr-5* | Glu | P | | [21] |
| *glr-6* | Glu | P | yes | |
| *glr-7* | Glu | P | yes | |
| *glr-8* | Glu | P | yes | |


1. Jospin, M. *et al.* A neuronal acetylcholine receptor regulates the balance of muscle excitation and inhibition in Caenorhabditis elegans. *PLoS Biol.* **7**, (2009).
2. Petrash, H. A., Philbrook, A., Haburcak, M., Barbagallo, B. & Francis, M. M. ACR-12 ionotropic acetylcholine receptor complexes regulate inhibitory motor neuron activity in Caenorhabditis elegans. *J. Neurosci.* **33**, (2013).
3. Towers, P. R., Edwards, B., Richmond, J. E. & Sattelle, D. B. The Caenorhabditis elegans lev-8 gene encodes a novel type of nicotinic acetylcholine receptor α subunit. *J. Neurochem.* **93**, (2005).
4. Touroutine, D. *et al.* acr-16 encodes an essential subunit of the levamisole-resistant nicotinic receptor at the Caenorhabditis elegans neuromuscular junction. *J. Biol. Chem.* **280**, (2005).
5. McKay, J. P., Raizen, D. M., Gottschalk, A., Schafer, W. R. & Avery, L. eat-2 and eat-18 are Required for Nicotinic Neurotransmission in the Caenorhabditis elegans Pharynx. *Genetics* **166**, (2004).
6. Fleming, J. T. *et al.* Caenorhabditis elegans levamisole resistance genes lev-1, unc-29, and unc-38 encode functional nicotinic acetylcholine receptor subunits. *J. Neurosci.* **17**, (1997).
7. Culetto, E. *et al.* The Caenorhabditis elegans unc-63 gene encodes a levamisole-sensitive nicotinic acetylcholine receptor α subunit. *J. Biol. Chem.* **279**, (2004).
8. Bamber, B. A., Beg, A. A., Twyman, R. E. & Jorgensen, E. M. The Caenorhabditis elegans unc-49 locus encodes multiple subunits of a heteromultimeric GABA receptor. *J. Neurosci.* **19**, (1999).
9. Beg, A. A. & Jorgensen, E. M. EXP-1 is an excitatory GABA-gated cation channel. *Nat. Neurosci.* **6**, (2003).
10. Jobson, M. A. *et al.* Spillover transmission is mediated by the excitatory GABA receptor LGC-35 in C. elegans. *J. Neurosci.* (2015) doi:10.1523/JNEUROSCI.4557-14.2015.
11. Keane, J. & Avery, L. Mechanosensory inputs influence Caenorhabditis elegans pharyngeal activity via ivermectin sensitivity genes. *Genetics* **164**, (2003).
12. Dent, J. A., Smith, M. M., Vassilatis, D. K. & Avery, L. The genetics of ivermectin resistance in Caenorhabditis elegans. *Proc. Natl. Acad. Sci. U. S. A.* **97**, (2000).
13. Cully, D. F. *et al.* Cloning of an avermectin-sensitive glutamate-gated chloride channel from Caenorhabditis elegans. *Nature* (1994) doi:10.1038/371707a0.
14. Horoszok, L., Raymond, V., Sattelle, D. B. & Wolstenholme, A. J. GLC-3: A novel fipronil and BIDN-sensitive, but picrotoxinin-insensitive, L-glutamate-gated chloride channel subunit from Caenorhabditis elegans. *Br. J. Pharmacol.* **132**, (2001).

776 15. Putrenko, I., Zakikhani, M. & Dent, J. A. A family of acetylcholine-gated chloride channel subunits in Caenorhabditis elegans. *J.*
777 *Biol. Chem.* **280**, (2005).
778 16. Takayanagi-Kiya, S., Zhou, K. & Jin, Y. Release-dependent feedback inhibition by a presynaptically localized ligand-gated anion
779 channel. *Elife* (2016) doi:10.7554/eLife.21734.
780 17. Feng, X. P., Hayashi, J., Beech, R. N. & Prichard, R. K. Study of the nematode putative GABA type-A receptor subunits: Evidence
781 for modulation by ivermectin. *J. Neurochem.* **83**, (2002).
782 18. Brockie, P. J., Mellem, J. E., Hills, T., Madsen, D. M. & Maricq, A. V. The C. elegans glutamate receptor subunit NMR-1 is required
783 for slow NMDA-activated currents that regulate reversal frequency during locomotion. *Neuron* **31**, (2001).
784 19. Kano, T. *et al.* Memory in Caenorhabditis elegans Is Mediated by NMDA-Type Ionotropic Glutamate Receptors. *Curr. Biol.* **18**,
785 (2008).
786 20. Rose, J. K., Kaun, K. R., Chen, S. H. & Rankin, C. H. GLR-1, a Non-NMDA Glutamate Receptor Homolog, Is Critical for Long-Term
787 Memory in Caenorhabditis elegans. *J. Neurosci.* **23**, (2003).
788 21. Zou, W. *et al.* Decoding the intensity of sensory input by two glutamate receptors in one C. elegans interneuron. *Nat. Commun.*
789 **9**, (2018).
790

791 Supplementary Table 1: **The list shows ligand identity and ion selectivity for LGICs in *C. elegans*.** Each
792 gene is assigned a polarity based upon its ion selectivity, this is shown in column 'Pos/Neg' as P: positive
793 (cation selectivity) or N: negative (anion selectivity). For orphan receptors the ligand and ion selectivity has
794 been predicted based on homology, this has been noted in the column 'Inferred' as 'yes'.

795

| Strain No. | Description |
|---|---|
| AQ4728 | him-5; IjEx1388[plgc-57::lgc-57::SL2GFP; punc-122:RFP] |
| PHX3594 | lgc-40(syb3594) |
| PHX3536 | lgc-57(syb3536) |
| PHX3562 | lgc-58(syb3562) |
| AQ4614 | IjEx1332[plgc-39(2kb)::lgc-39::SL2 GFP; punc-122::RFP] |
| AQ4427 | IjEx1254[plgc-40(2kb)::mKate2::gpd-23'UTR; unc-122::gfp] |
| AQ4423 | IjEx1252[plgc-57(2kb)::mKate2::gpd-23'UTR; unc-122::gfp] |
| AQ4377 | IjEx1242[plgc-39(2kb)::mKate2::gpd-23'UTR; unc-122::gfp] |
| AQ4428 | IjEx1255[plgc-58(2kb)::mKate2::gpd-23'UTR; unc-122::gfp] |
| AQ5072 | IjEx1562[plgc-46::GFP::gpd-2UTR; punc-122::RFP] |
| OH15262 | "NeuroPAL" otEx7057 |
| AQ4657 | lgc-39(lj121) |
| AQ4850 | NeuroPal(otEx7057); IjEx1453 [plgc-33::lgc-33::SL2 GFP; punc-122::RFP] |
| AQ4837 | NeuroPal(otEx7057); IjEx1449 [plgc-34::lgc-34::SL2 GFP;unc-122::RFP] |
| AQ4529 | him-5(e1490); IjEx1299[plgc-48::gDNA lgc-48 3'UTR::SL2 mKate2;punc-122::GFP] |
| AQ4928 | IjEx1498 [plgc-47(2kb)::lgc-47::SL2 GFP; unc-122::RFP] |
| AQ4849 | NeuroPal(otEx7057); IjEx1453 [plgc-49::lgc-49::SL2 GFP; unc-122::RFP] |

796 Note:
797 *lgc-57* previously called *ggr-1*
798 *lgc-58* previously called *ggr-2*
799
800 Supplementary Table 2: **List of *C. elegans* strains used in this study**

801

| **Description** | **Sequence** |
|---|---|
| ggr-1 gene F | GGGGACAAGTTTGTACAAAAAAGCAGGCTTAatgcattccttattcctgaaaattctgatatacag |
| ggr-1 gene R | GGGGACCACTTTGTACAAGAAAGCTGGGTTttaaagcaaaagttcaggggaattgct |
| ggr-2 gene F | GGGGACAAGTTTGTACAAAAAAGCAGGCTTAatgcttcttgtctcttcaatattcttattactgtacag |
| ggr-2 gene F | GGGGACCACTTTGTACAAGAAAGCTGGGTTatgggatgtgaaatatgaaaaattatacacttggtt |

| | |
|---|---|
| ggr-2 promoter F | GGGGACAACTTTGTATAGAAAAGTTGTAccccggaaagcatctggtaaac |
| ggr-2 promoter R | GGGGACTGCTTTTTTGTACAAACTTGTaatgccgtcgtggtaagacgttatagttgac |
| lgc-39 promoter F | GGGGACAACTTTGTATAGAAAAGTTGTAatcgttttgtgggacacctttagg |
| lgc-39 promoter R | GGGGACTGCTTTTTTGTACAAACTTGTcgatgattcacatcagggatgcttcaac |
| lgc40_gene_F | GGGGACAAGTTTGTACAAAAAAGCAGGCTTAatcgaaactatgagccaactaaaatccaaa |
| lgc40_gene_R | GGGGACCACTTTGTACAAGAAAGCTGGGTTatacataataatttattttcaaattaaaatggctaatatcatcatcgt |
| plgc40_promoter_F | GGGGACAACTTTGTATAGAAAAGTTGTAatacgggtcattcttgccct |
| plgc40_promoter_R | GGGGACTGCTTTTTTGTACAAACTTGTctgaaattccaaaatctggcgtcaattagattga |
| lgc41_gene_F | GGGGACAAGTTTGTACAAAAAAGCAGGCTTAatgaaaaagtactggtcaactctacattgt |
| lgc41_gene_R | GGGGACCACTTTGTACAAGAAAGCTGGGTTctatttatcaattggagtttttgtatatactaaatagtaccaccag |
| plgc41_promoter_F | GGGGACAACTTTGTATAGAAAAGTTGTAtgccataatctgggtgatttagataagttctct |
| plgc41_promoter_R | GGGGACTGCTTTTTTGTACAAACTTGTcctctattctatattgtgaaaaaattcgttgttcaaaaatcctgc |
| lgc45c_P221_F | GGGGACAAGTTTGTACAAAAAAGCAGGCTTAatggactacaatctatcgactgatgacttttgaggagt |
| lgc45ac_P221_R | GGGGACCACTTTGTACAAGAAAGCTGGGTTgacaagacagccacaaaaaaataacaacg |
| lgc45a_P221_F | GGGGACAAGTTTGTACAAAAAAGCAGGCTTAatgccacgtcataaccatttcatcc |
| plgc45c_P4P1r_F | GGGGACAACTTTGTATAGAAAAGTTGTAaacacgcttagcggaccaaa |
| plgc45c_P4P1r_R | GGGGACTGCTTTTTTGTACAAACTTGTggccttgtagcttgtgtcaatccataaaac |
| plgc45a_P4P1r_F | GGGGACAACTTTGTATAGAAAAGTTGTAgttttccgcccatcccca |
| plgc45a_P4P1r_R | GGGGACTGCTTTTTTGTACAAACTTGTtttgtgacgggtgcatctggaatt |
| plgc43short_P4P1r_F | GGGGACAACTTTGTATAGAAAAGTTGTAattgaatggttttaaactaaacacaaaagcctg |
| plgc43short_P4P1r_R | GGGGACTGCTTTTTTGTACAAACTTGTttttcatccatttttttaggtcatagattgtagaatatagtagagg |
| lgc44_P221_F | GGGGACAAGTTTGTACAAAAAAGCAGGCTTAatgtctcttcttatctctatttctcttctttttctaatatttcc |
| lgc44_P221_R | GGGGACCACTTTGTACAAGAAAGCTGGGTTgttcatacacatttattcaatttttaatacactttctctcatctcc |
| plgc44_P4P1r_F | GGGGACAACTTTGTATAGAAAAGTTGTAagcgaattggagcttttgct |
| plgc44_P4P1r_R | GGGGACTGCTTTTTTGTACAAACTTGTcgattgatgtcttctacattgaaatcagaaatagagt |
| lgc42_P221_F | GGGGACAAGTTTGTACAAAAAAGCAGGCTTAatgacttctaatcgatggcttctattttttttattgt |
| lgc42_P221_R | GGGGACCACTTTGTACAAGAAAGCTGGGTTtcagtccattaatgggggttctcgt |
| plgc-42_P4P1r_F_v2 | GGGGACAACTTTGTATAGAAAAGTTGTAggcgtgtcctggaaaatgtgt |
| plgc-42_P4P1r_R_v2 | GGGGACTGCTTTTTTGTACAAACTTGTtttaatccaaaacgtcaactcaaaacgggg |
| gRNA1_lgc39_sens | TTGgtaattgcgaataataccga |
| gRNA1_lgc39_anti | AACtcggtattattcgcaattac |
| lgc39_3hom_F | GGCTGCTCTTCgACGggatccgacctgaatcgg |
| lgc39_3hom_R | GGGTGCTCTTCgTACacgacctttttggaagttaatgga |
| lgc39_5hom_F | GGCTGCTCTTCgTGGtgagattttggaagcaatttcc |
| lgc39_5hom_R_noPAM | GGGTGCTCTTCgCATttcggtattattcgcaattactgg |

| | |
|---|---|
| ggr2_GFP_F | gtaccggcggtagtgGAAGAAGTTTGGGCAGAACAAAAAGAAAC |
| ggr2_GFP_R | aacaattcttctcctttacTCATTTGGGCCTCAGCGTCTT |
| ggr1_GFP_F | gtaccggcggtagtgGTGGCGCAGTACAGGGAG |
| ggr1_GFP_R | aacaattcttctcctttacTCATCATGTCATGTACTTGCTCCGAGAG |
| lgc40_GFP_F | gtaccggcggtagtgGGAGCGGCCCGAGATATAGAC |
| lgc40_GFP_R | aacaattcttctcctttacTCATGAACAATGTTGAGAGAGCAGTGTCG |
| lgc39_GFP_KSM_F | ggcggtagtGGATCCGACCTGAATCGGAATAAAAAATCTCAGCA |
| lgc39_GFP_KSM_R | ctttacTCATCTCGGTATTATTCGCAATTACTGGCTTGTTG |

Supplementary Table 3: **List of primers used in this study**

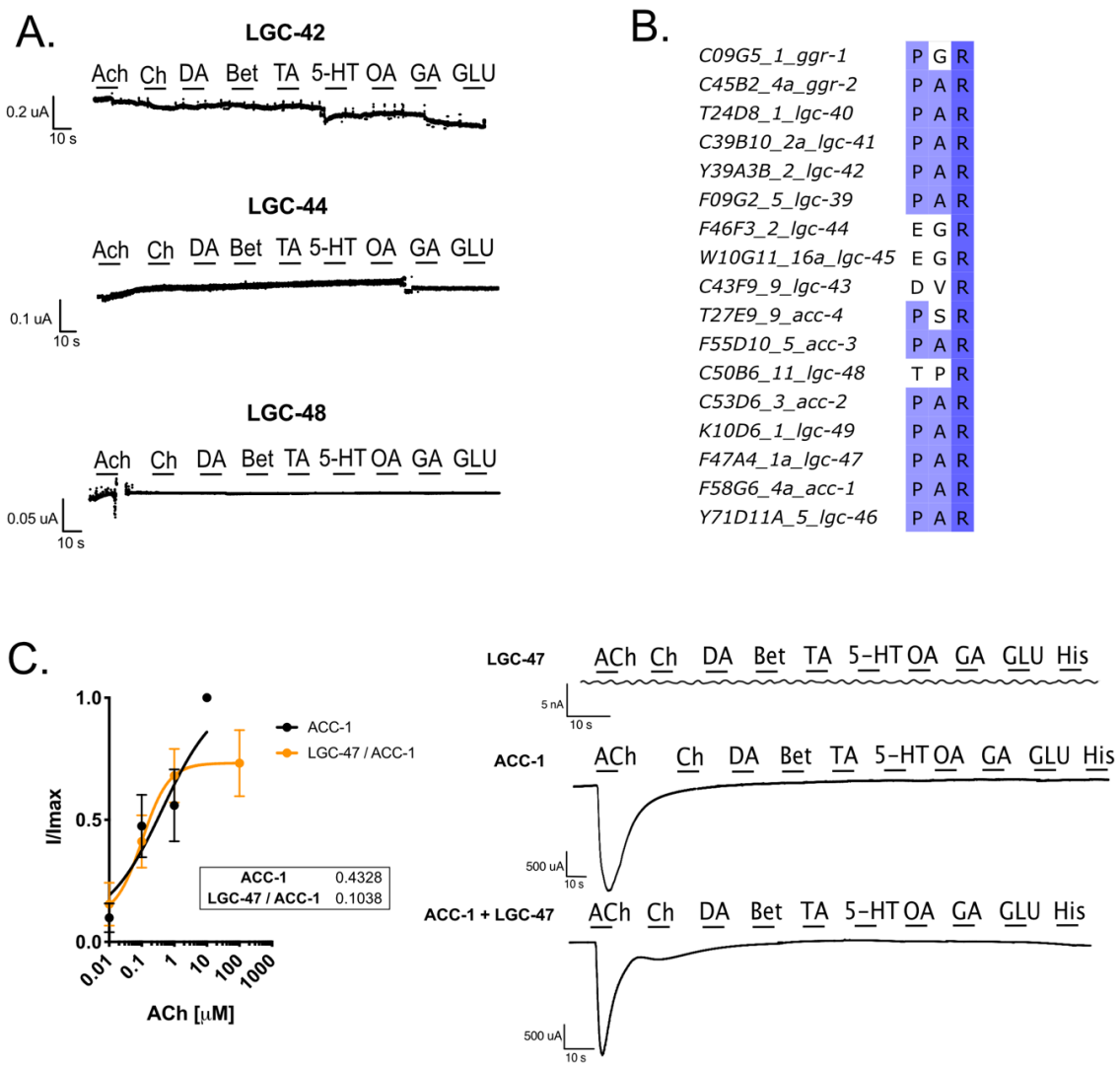


Supplementary Figure 1: **Negative traces for still orphan LGICs, representative ion selectivity curves and channel kinetics**

A. Continuous TEVC traces from oocytes clamped at -60mV expressing LGC-42, LGC-44, and LGC-48, exposed to 10s of a panel of ligands. B. Alignment of PAR motifs for channels in the diverse and ACC groups. C. LGC-

809 47 and ACC-1 do not form a heteromeric channel in *Xenopus* oocytes. Left: Acetylcholine-induced dose response
810 curves for oocytes expressing ACC-1 alone, or in combination with LGC-47. Error bars represent SEM of 7-12
811 oocytes per construct, insert shows $EC_{50}$ values. Right: Continuous TEVC traces from oocytes clamped at -60mV
812 expressing LGC-47, ACC-1, or a combination, exposed to 10s of a panel of ligands. Note that the small changes
813 in current seen in the traces are attributed to recording and perfusion artefacts.

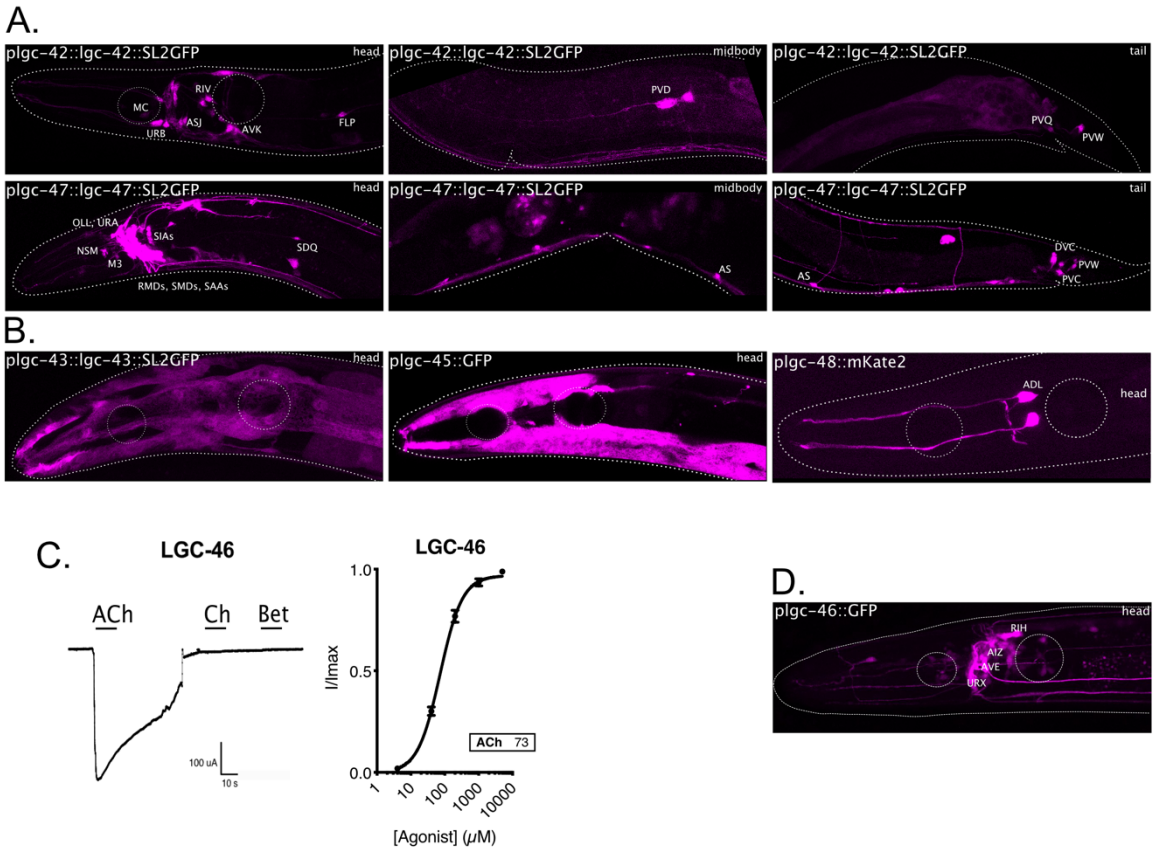


814

815 <u>Supplementary Figure 2:</u> **Expression patterns of still orphan LGICs and LGC-46 characterisation**

816 A-B. Expression of fluorescent reporters for still orphan LGCIs, head body and tail are shown for *lgc-42* and *lgc-*
817 *47* (A), head only is shown for *lgc-43*, *lgc-45* and *lgc-48* (B). C. Acetylcholine-induced dose response curve,
818 continuous trace, and expression pattern of LGC-46. Error bars represent SEM of 6 oocytes. Insert shows $EC_{50}$.
819 Dose response curves for GFP tagged LGICs in response to their major activating ligands. Error bars represent
820 SEM of 4-5 oocytes per construct, inserts show $EC_{50}$. D. Expression of fluorescent reporters for plgc-46 shows a
821 broad neuronal expression pattern with expression in e.g., AIZ, RIH and AVE neurons.

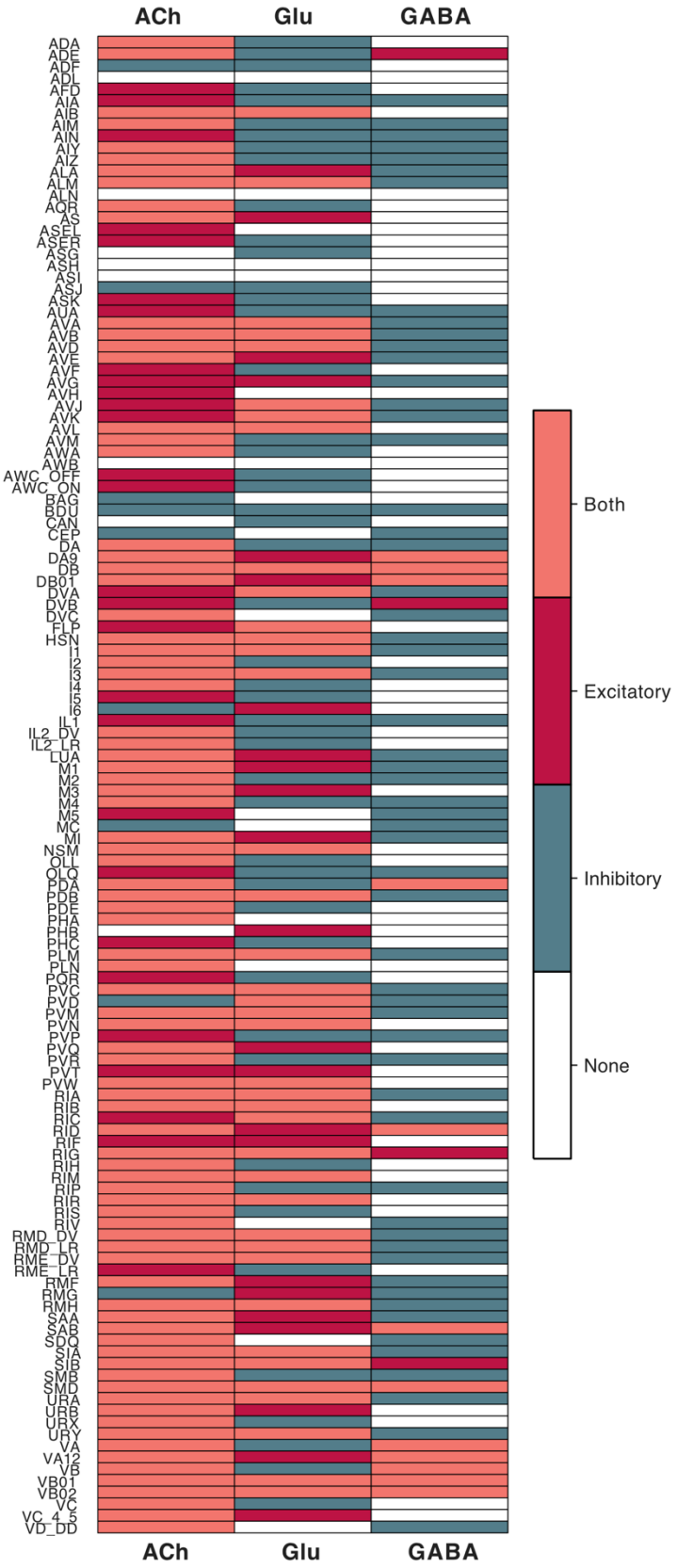


822

823 Supplementary Figure 3: **Binary heatmap of synaptic sign prediction for the three major**

824 **neurotransmitters; ACh, glutamate and GABA**

The heatmap shows the summed expression level of all LGICs in *C. elegans* per neural class and neurotransmitter, a net sum of excitatory channels is displayed in red, inhibitory in green, equal expression in peach and no expression of LGICs in white.

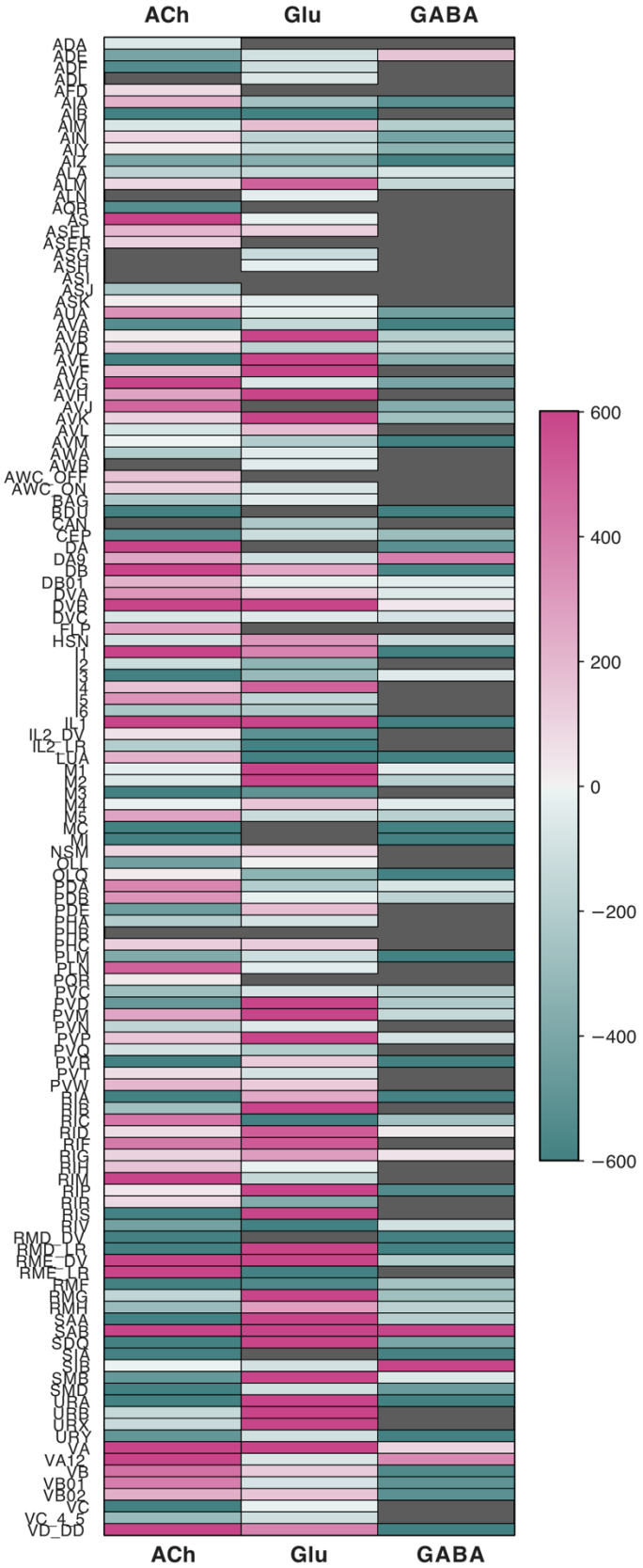

Supplementary Figure 4: **Expression heatmap for the three major neurotransmitters**

The heatmap shows the summed expression level, and ion selectivity, for LGICs separated by transmitter (ACh, glutamate and GABA) and neural class. Net excitatory channel expression is represented in pink and inhibitory in green.

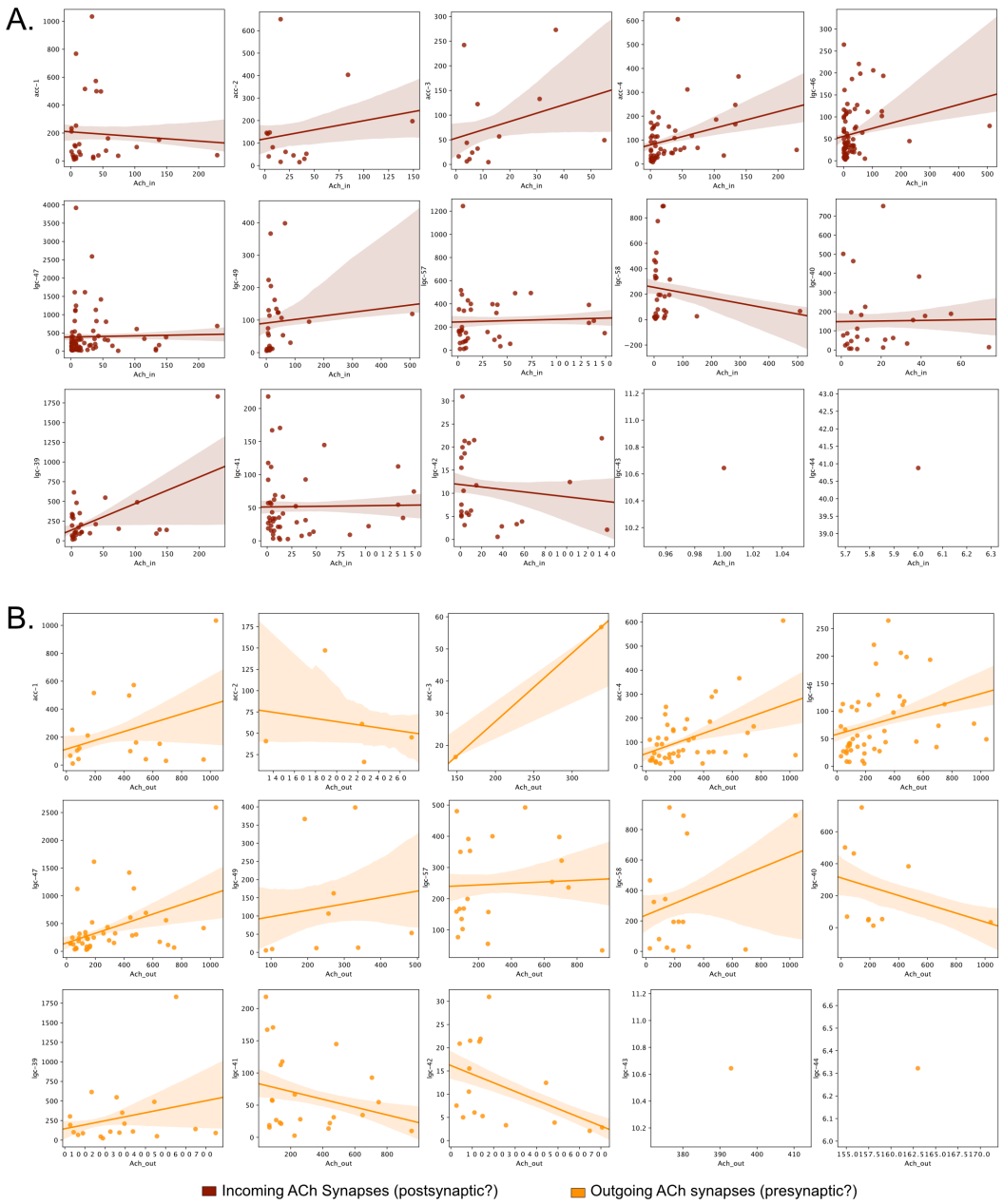


Supplementary Figure 5: **Correlation graphs between cholinergic synapses and expression of selected LGICs**

Scatter plots showing gene expression level vs total number of incoming cholinergic synapses (red) and outgoing cholinergic synapses (orange). Lines fit using relplot with shaded areas representing the standard error of the line fit.

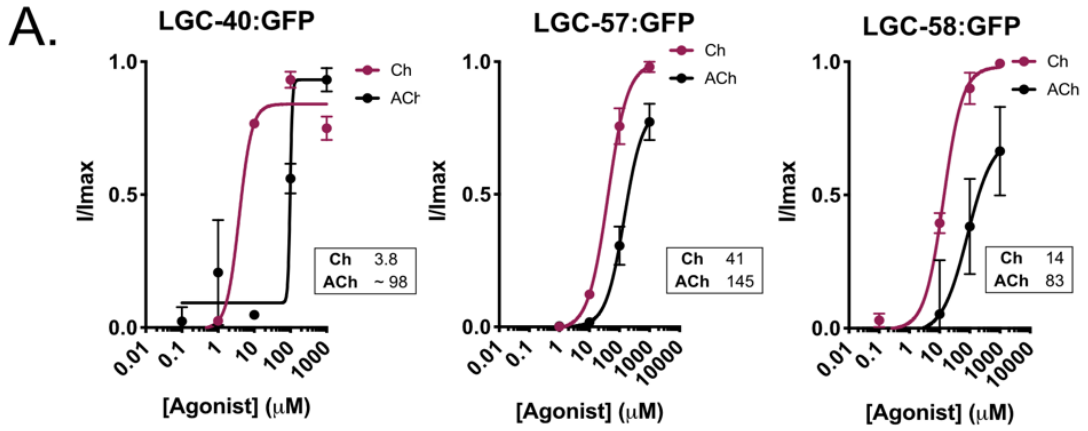


839

840 Supplementary Figure 6: **GFP tagging of LGICs does not influence channel function**

841 Acetylcholine- or choline-induced dose response curves for oocytes expressing GFP tagged versions of LGC-40,

842 LGC-57 and LGC-58 shows that $EC_{50}$ values are not influenced by the insertion of the GFP tag. Error bars

843 represent SEM of 7-12 oocytes per construct, insert shows $EC_{50}$ values.